JGR Oceans

RESEARCH ARTICLE
10.1029/2022JC019609

Episodic Summer Chlorophyll-a Blooms Driven by Along-Front Winds at Aotearoa's Southeast Shelf Break Front

Erik E. Johnson[1], Sutara H. Suanda[2], Stephen R. Wing[1], Kim I. Currie[3], and Robert O. Smith[1]

[1]Department of Marine Science, University of Otago, Dunedin, New Zealand, [2]Department of Physics and Physical Oceanography, University of North Carolina Wilmington, Wilmington, NC, USA, [3]NIWA, Dunedin, New Zealand

Key Points:

- Remotely-sensed summer chlorophyll-a concentrations are enhanced at the southeast shelf break of Aotearoa/NZ following upfront wind stress
- Surface chlorophyll-a was reduced at the shelf break following downfront wind stress, despite relatively elevated nitrate concentrations
- Ekman restratification by upfront wind stress is proposed as a likely mechanism for episodic summer shelf break chlorophyll-a enhancements

Supporting Information:

Supporting Information may be found in the online version of this article.

Correspondence to:

E. E. Johnson,
erik.johnson@postgrad.otago.ac.nz

Citation:

Johnson, E. E., Suanda, S. H., Wing, S. R., Currie, K. I., & Smith, R. O. (2023). Episodic summer chlorophyll-a blooms driven by along-front winds at Aotearoa's southeast shelf break front. *Journal of Geophysical Research: Oceans*, *128*, e2022JC019609. https://doi.org/10.1029/2022JC019609

Received 22 DEC 2022
Accepted 29 JUN 2023

Author Contributions:

Conceptualization: Robert O. Smith
Data curation: Kim I. Currie
Methodology: Robert O. Smith
Resources: Kim I. Currie
Supervision: Sutara H. Suanda, Stephen R. Wing, Robert O. Smith
Writing – review & editing: Sutara H. Suanda, Stephen R. Wing, Kim I. Currie, Robert O. Smith

Abstract This study investigates the influence of along-front wind forcing on chlorophyll-a (Chl-a) at the Otago Shelf Break (OSB) in southeast Aotearoa/New Zealand using remotely-sensed and in situ data. Summer wind stress over the OSB was shelf-aligned, oscillating between upfront and downfront. Surface Chl-a concentrations along the OSB were shown to increase episodically (≤10 days duration) following upfront wind stress. This response occurred over most of the 350 km long shelf break, and was most intense north of the Otago Peninsula. Peak Chl-a enhancement at the shelf break occurred following periods of upfront winds, exhibiting a lagged response of approximately 5 days. Moored thermistor data indicated that upfront wind events were followed by increased thermal stratification over the mid-shelf, whereas downfront wind events were followed by a well-mixed water column. In situ temperature, salinity, and nutrient measurements suggested an offshore movement of the surface expression of the front following upfront winds, and a reduction in nitrate over the shelf break. From these observations a model of Ekman restratification driven by upfront winds is proposed for this system, wherein off-shelf Ekman transport converts strong horizontal isopycnal gradients at the shelf break front into vertical stratification. This stratification holds phytoplankton in the upper water column, allowing increased access to light, which is marked by the increased drawdown of nitrate at the shelf break. Downfront winds break down this stratification, move the shelf break front onshore, and mix phytoplankton through the water column, reducing the surface expression of chlorophyll.

Plain Language Summary The southeast coast of Aotearoa/New Zealand has a relatively near-shore "shelf break," the area where shallow continental shelf seas (<200 m) slope steeply toward the deeper ocean (>1,000 m). Here lighter shelf waters meet more-dense off-shelf waters, forming a "shelf break front." Satellite images show large phytoplankton blooms occurring over the whole shelf break front in summer months, but researchers have not yet explored the factors that cause these short-lived events. Understanding phytoplankton patterns and the ocean processes driving them is key to our knowledge of this ecosystem, which is home to endangered marine species and commercial fisheries. This study uses satellite images of chlorophyll-a and winds, in tandem with in-person ship and mooring data to explore how winds influence chlorophyll-a at this front. Winds that are aligned with the shelf break (here southwest/northeast) are focused on due the cross-shelf movement they can generate. This study finds that northeast winds cause increases in chlorophyll-a at the front, which we believe to result from increased water column stability when light waters move over dense waters. This stratification provides a near-surface layer with abundant light. During southwest winds, this stability is believed to be broken down, mixing phytoplankton away from the surface.

1. Introduction

1.1. Productivity at Shelf Break Fronts

Productivity and high biodiversity are generally associated with the shelf seas bordering continental landmasses (Costello & Chaudhary, 2017). These regions draw the majority of global fishery landings (Watson et al., 2004) and intersect with significant anthropogenic pressures despite their relatively small footprint. Identifying oceanographic processes that support the primary productivity underpinning shelf ecosystems improves our ability to model and understand both the past and future of marine ecosystem dynamics. At shelf margins, horizontal and vertical mixing processes associated with shelf break fronts are critical in modifying shelf temperature, salinity, and nutrient distributions, due to the often significant gradients between shelf and open regions (Brink, 2016).

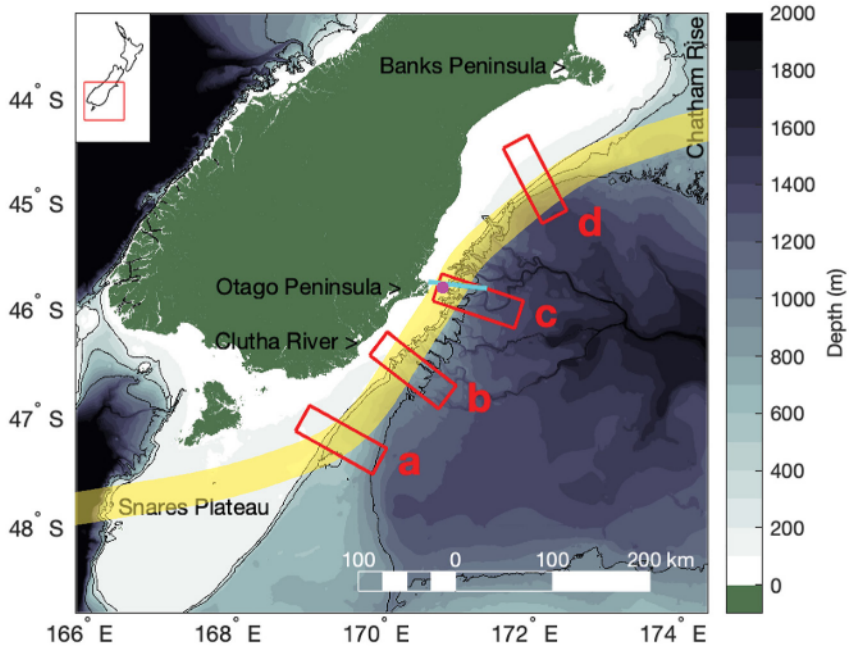

Figure 1. Bathymetry of the Otago Shelf Break region. Red boxes show transects a through d. General position of the subtropical front is indicated in yellow, location of Munida Transect is in cyan, magenta dot represents position of mooring deployment, the 200, 500 and 1,000 m isobaths are outlined in black.

These forces modify stratification and nutrient availability; conditions that can support or suppress primary productivity.

Spring and autumn seasonal bloom cycles are typical of shelf seas, and have been strongly linked to the timing of stratification/destratification in the presence of sufficient insolation (Childers et al., 2005; Ferreira et al., 2015; Hopkins et al., 2021; Xu et al., 2011). At shelf break fronts, these seasonal primary productivity patterns are further affected by transient processes (wind stress, eddies, frontal meanders) that interact with the unique hydrography of these regions and generate significant sub-seasonal variability (Franks & Walstad, 1997; Longhurst, 2007). Studies of the Mid-Atlantic Bight (Oliver et al., 2022) and Patagonian Shelf (Carranza et al., 2017) demonstrate that blooms at shelf break fronts are not always accompanied by blooms over the shelf, emphasizing the presence of independent mechanisms driving Chl-a enhancement at the shelf break.

1.2. The Otago Shelf Break

The Otago Shelf Break (OSB) region (Figure 1) off the southeast coast of Aotearoa/New Zealand (ANZ) is characterized by a relatively narrow shelf (approximately 20 km off Ōtākou/the Otago Peninsula) and the presence of three distinct water masses; near-shore neritic water primarily sourced from the Mata-Au/Clutha River (ANZ's largest river by discharge), freshwater-modified subtropical water (STW), and subantarctic water (SAW) beyond the shelf break (Jillett, 1969). Along the OSB, STW and SAW form a well defined front that is bathymetrically locked near the 500 m isobath, moving onshore/offshore in the summer/winter and meandering more frequently to the north (Hopkins et al., 2010). Here the front is associated with a fast flowing shelf break jet (average speed >0.2 m/s), known as the Southland Current (Chiswell, 1996). This frontal jet follows northeast from the bottom of Te Wai Pounamu/the South Island toward the Chatham Rise where it detaches from the slope and deflects to the east as isobaths diverge (Chiswell, 1996; Vincent et al., 1991). The shelf break front can be recognized by strong gradients in temperature, salinity, and nutrients where warm, salty, high-silicate, macronutrient-poor STW meets cool, fresh, low-silicate, macronutrient-rich SAW water (Boyd et al., 1999; Currie et al., 2011; Jones et al., 2013). This region's ecosystem supports several endemic and endangered marine species (Augé et al., 2012), in addition to significant commercial fisheries (Leathwick et al., 2006), highlighting the need to understand mechanisms driving phytoplankton variability along the OSB.

Early remotely-sensed studies of this region (Murphy et al., 2001) identified maximum monthly averaged surface chlorophyll-a (Chl-a) concentrations (>1 mg/m^3) occurring in the subtropical front regions to the east and west of ANZ from 3 years of 9 km binned SeaWiFS monthly composite data. Though the authors observed relative enhancement year-round at the subtropical front east of ANZ, they noted distinct peaks in Chl-a concentration in February-March, and September. Mixing of limiting nutrients across STW and SAW was suggested as the potential source of observed productivity, but the specific mechanisms of exchange were not explored. Boyd et al. (2004) similarly noted enhanced Chl-a concentrations over the Chatham Rise from 5 years of monthly to 8-day SeaWiFS composites. The notion of cross-shelf Ekman transport across the front was investigated as a potential mechanism of nutrient supply (particularly iron) to fuel the blooms, and the authors found comparable volumes of Ekman transport to those required to sustain these blooms. However, the timing of Chl-a enhancements did not coincide with the timing of the largest Ekman transport, which led the authors to rule out transport or wind-driven mixing as the sole source of nutrients. This work was expanded upon by Chiswell et al. (2013), utilizing further years of SeaWiFS data. The patterns found within the longer time series (13 years) largely agree with previous studies, and the authors connect timing of seasonal bloom onset to the spring/autumn with reduction/increase of wind stress in the absence of convective cooling. These remotely-sensed studies identified enhanced Chl-a associated with the subtropical front surrounding ANZ and established monthly climatologies, although the temporal and spatial scales considered prevented analysis of sub-monthly variability in near-shore regions of the subtropical front, such as the OSB.

The most in-depth analysis of primary productivity over a portion of the OSB was conducted by Jones et al. (2013) along a 60 km transect extending off the Otago Peninsula (cyan line, Figure 1). This transect sampled temperature, salinity, nutrients, and Chl-a bi-monthly from the coast to beyond the shelf break, covering neritic, STW, and SAW masses. Using transect data collected from July 2009 to November 2010, the authors found peak productivity in the spring and summer seasons (October–March), generally constrained to neritic and STW inshore of the shelf break. Chl-a concentrations observed during these cruises rarely exceeded 1 mg/m^3, making locally elevated Chl-a more comparable to the open-ocean subtropical-frontal zone than other near-coast boundary current systems, despite the narrowness of the shelf and presumed supply of terrestrial nutrients (Jones et al., 2013). Seasonal blooms in NW and STW were found to be associated with near-zero nitrate concentrations, suggesting that phytoplankton in the region is primarily nitrate limited; however near-depletion in silicate concentrations (<1 μmol/L) along the entire transect also indicated the importance of silicate in sustaining productivity, particularly further offshore in macronutrient rich SAW (Jones et al., 2013).

Daily ocean color images capture sporadic periods of elevated Chl-a concentrations spanning the entire OSB front (Figure 2). An example bloom during December 2018 saw remotely-sensed Chl-a concentrations approaching 4 mg/m^3 for most of the shelf break, intensifying and fading between the 29th of November and the 17th of December. Chl-a concentrations observed during this event are comparable to the largest values seen for this region in prior studies (Boyd et al., 2004; Chiswell et al., 2013; Jones et al., 2013), though previous work has not described such transient shelf break enhancement events. Because these blooms occur on sub-monthly timescales, the characteristics of their frequency, intensity, or spatial extent cannot be captured by monthly composites or bi-monthly snapshots (Boyd et al., 2004; Chiswell et al., 2013; Jones et al., 2013; Murphy et al., 2001). Furthermore, the oceanographic processes occurring over the duration of these sporadic bloom events have yet to be explored. Studies in comparable shelf break regions have consistently identified a relationship between along-front wind (AFW) forcing and Chl-a enhancement at shelf break fronts (Carranza et al., 2017; Oliver et al., 2022; Siedlecki et al., 2011; Xu et al., 2011). The OSB experiences synoptic-scale wind stress variability that is strongly shelf-aligned as a result of topographic steering around ANZ (Chiswell, 1996; Jones et al., 2013; Kidson, 2000; Sturman et al., 1984), making this region a unique natural laboratory for studying the impact of upfront/downfront (northeasterly, against the flow of the frontal current/southwesterly, with the flow of the frontal current for the OSB) wind forcing on shelf break primary productivity.

1.3. Influence of Winds on Shelf Break Productivity

The current study focuses on three major AFW mechanisms which may impact episodic blooms at the OSB region: entrainment (Carranza & Gille, 2015), on-shelf movement and mixing of slope waters from oscillating AFW stress (Siedlecki et al., 2011), and Ekman restratification in the upper water column (Oliver et al., 2022). The development and oceanic response of these mechanisms occur within the duration of synoptic weather events

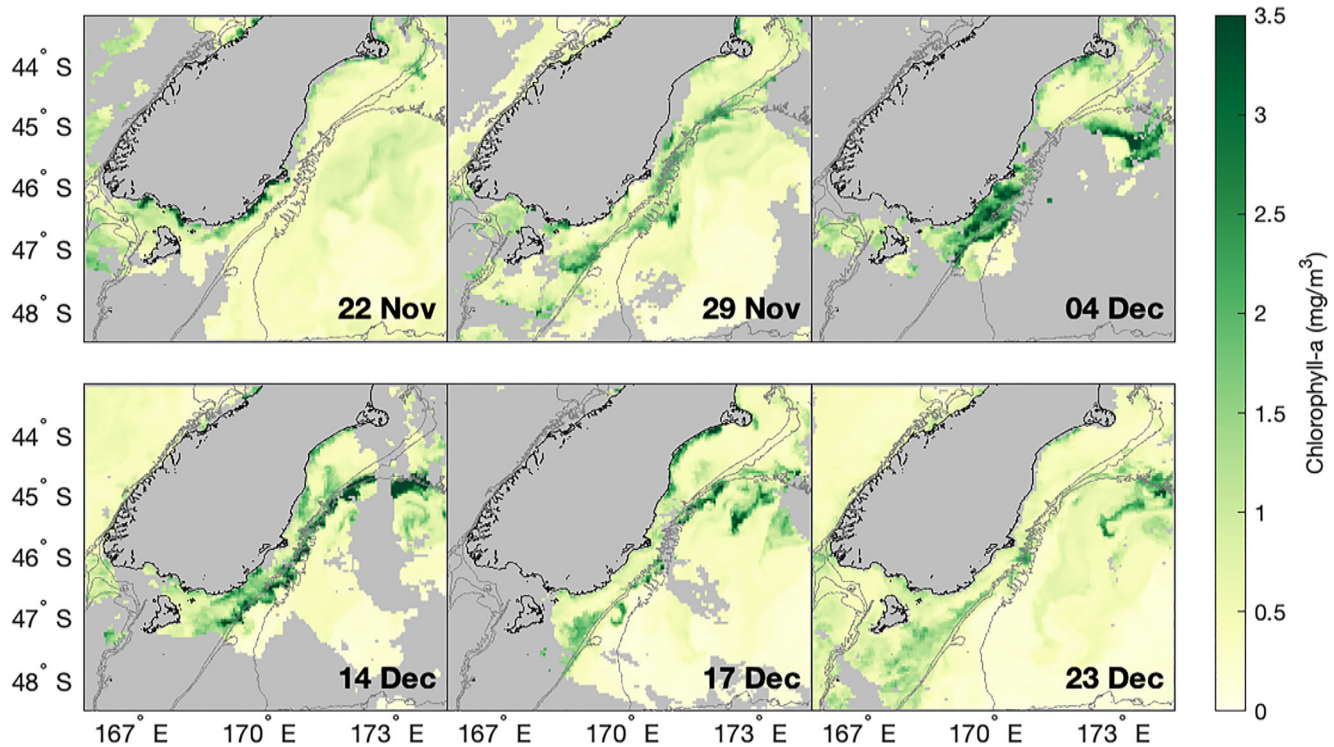

Figure 2. Sequence of daily chlorophyll-a images showing bloom evolution at the Otago Shelf Break in Austral Summer of 2018. 0 m isobath is outlined in black, the 200, 500 and 1000 m isobaths are outlined in gray.

(<14 days) (Franks, 2001; Siedlecki et al., 2011), facilitating conditions conducive to phytoplankton growth on similar timescales to observed OSB bloom events. The impacts of AFW forcing on stratification and cross-front mixing of nutrient rich water are the primary considerations relevant to phytoplankton growth for this study; impacts of these processes on community structure and grazing rates are beyond the intended scope.

Wind driven vertical entrainment over the shelf is well established as a mechanism relevant for bloom onset in shelf seas and the open ocean (Carranza et al., 2017; Chiswell et al., 2013; Ferreira et al., 2015; Long et al., 2012), and has been connected to the timing of seasonal bloom initiation on ocean-wide scales in both the northern and southern hemisphere (Carranza & Gille, 2015; Ferreira et al., 2015). Stratification can be broken down by significant wind stress, allowing phytoplankton in the surface layer to access entrained nutrients from beneath the euphotic zone. How productivity responds to wind driven entrainment is not trivial, however, as turbulent mixing can dilute phytoplankton concentrations at the surface, reduce access to photosynthetically active radiation via deepening of the mixed layer, and affect water clarity (Carranza & Gille, 2015; Ferreira et al., 2015). To further complicate wind-driven mixing, the presence of a shelf break front alters the effective wind stress and isopycnal structure, potentially generating intensified entrainment responses compared to those at the shelf, especially following downfront wind stress (Thomas & Lee, 2005).

Isopycnal adjustment in response to oscillating upfront/downfront wind forcing has consistently been shown in idealized two-dimensional models to entrain nutrients and generate primary productivity (Franks & Walstad, 1997; Siedlecki et al., 2011; Whitt et al., 2017). In numerical simulations of a shelf break front, Siedlecki et al. (2011) show that upfront wind stress induces Ekman transport which moves buoyant shelf waters off-shelf at the surface. This movement is compensated by moving the foot of the front on-shore, drawing cooler, nutrient-rich, deep slope waters onto the shelf. Isopycnals steepen when winds shift downfront, mixing shelf waters downward and entraining the onwelled nutrient-rich slope water into the euphotic zone; leading to a phytoplankton bloom on the shelf side of the front in the model. This nutrient supply mechanism was highlighted by Carranza et al. (2017) as a potential mechanism influencing Chl-a enhancement observed at the Patagonian shelf break front following periods of downfront winds. Modelling by Franks and Walstad (1997) also shows that oscillating AFW stress can generate enhanced productivity in an open-ocean front without reliance on onwelled slope water. In the

authors' two dimensional model, downfront winds steepen isopycnals, and create onshore movement of dense waters over the buoyant side of the front. This causes overturning, the deepening of mixed layers, and entrainment of nutrients on the light side of fronts. Chlorophyll-a "patches" are then established when upfront wind stress flattens isopycnals and reduces vertical mixing, allowing stratification to develop at the front (Franks & Walstad, 1997). Numerical models from Whitt et al. (2017) further show that oscillating winds with both high and low-frequency components can result in anomalously deep mixed layers in open-ocean fronts. This enhanced mixing produces increased nutrient entrainment and productivity on the less dense side of fronts in models with low (8-day) and high (1.6–0.5 days) frequency wind components, lagging maxima in downfront stress by 2 days (Whitt et al., 2017).

Ekman-restratification occurs when upfront wind stress generates offshore Ekman transport, moving lighter waters over the dense side of fronts and slumping isopycnals from vertical to horizontal. This process has been put forth as a driver of transient frontal blooms during springtime in the Ross Sea (Long et al., 2012), where weakly stratified waters can experience localized stratification over the shelf break following upfront winds, providing phytoplankton with sustained light access in nutrient replete waters. The occurrence of similar episodic spring blooms following periods of upfront stress has also been recently observed in the Mid-Atlantic Bight, supported by two-dimensional ROMS simulations that generated phytoplankton blooms and density patterns consistent with Ekman-restratification (Oliver et al., 2022). These enhancement events following Ekman restratification are largely associated with light-limited waters in spring following deep winter mixing (Lévy et al., 2000; Long et al., 2012; Oliver et al., 2022); however, it is possible that upfront wind stress can generate similar shelf break front stratification in the summer provided frontal isopycnals are sufficiently vertical. Ekman restratification following upfront wind stress potentially contributes to elevated remotely-sensed Chl-a concentrations observed offshore of the Patagonian shelf break in summer months (Carranza et al., 2017), although this mechanism has yet to be explored as a driver of episodic summer blooms at the shelf break.

1.4. Study Objectives

The present study seeks to test the connection between AFW mechanisms and episodic bloom events observed at the OSB. Section 2 describes remotely-sensed and in situ data sources, as well as the methodology used for composite and event analysis. Section 3.1 presents median Chl-a climatologies in order to evaluate the magnitude of seasonal patterns and areas of high variability. Seasonal distributions for wind direction and magnitude are regionally averaged over the OSB and used to characterize the predominant winds for this system. Section 3.2 identifies periods of elevated/reduced shelf break Chl-a from remotely-sensed images, and characterizes the preceding wind forcing. From this, OSB productivity is composited by periods of varying wind stress to quantify the intensity and variability of any patterns observed. This is complemented by Section 3.3, which analyses in situ measurements of Chl-a, temperature, salinity, and nitrate from both ship-based and moored thermistor observations in terms of wind forcing. This offers further insight into the response of the frontal system to variable wind stress, and adds additional context to observed remotely-sensed patterns. Ultimately, potential AFW mechanisms influencing OSB productivity are considered.

2. Data and Methods

2.1. Data

2.1.1. Remotely-Sensed Data

Remotely-sensed Chl-a fields were acquired from version 5.0 of the European Space Agency's (ESA) Ocean Color Climate Change Initiative (OC-CCI+) (Sathyendranath et al., 2021). Daily data are available from 1997 to 2021 on an approximately 4 km grid. This data set (hereafter ESACCI) blends bias-corrected and band-shifted ocean colour imagery from SeaWiFS, MODIS, VIIRS, OLCI, and MERIS satellite platforms into a single Chl-a product. A series of weighted algorithms are used to maximize performance for 14 different water classes, particularly improving performance in near-shore waters (Sathyendranath et al., 2019). This data product has yet to be validated for the OSB, so comparison against in situ measurements was undertaken (see Supporting Information S1) to evaluate accuracy. This is of particular importance for a region with significant freshwater influence, where erroneous Chl-a values are more likely (Sathyendranath et al., 2019) due to riverine sediment. Agreement between ESACCI and in situ data was strong ($R^2 = 0.72$) when omitting data 15 km from the coast

(Figure S1 in Supporting Information S1). Therefore, any ESACCI pixels within 15 km of the coast were masked in subsequent analysis.

Hourly 10 m wind speeds (u and v components) from the European Centre for Medium-Range Weather Forecasts' fifth generation re-analysis product (hereafter ERA5) were used for computing the wind stress over the OSB. The product assimilates data from over 200 satellite platforms and in situ observations to produce a global atmospheric hindcast at 31 km resolution (Hersbach et al., 2020). Data are available from 1979-present, although only data from 1997-onward are used to correspond to the availability of ESACCI images. Validation against in situ data is not pursued here due to the absence of ocean-based wind measurements, and potentially significant topographic effects on inland weather stations available for comparison (Chiswell, 1996). However, ERA5 validation against buoy winds in the northern Pacific and Atlantic show good agreement (Sharmar & Markina, 2020). The large spatial scales (>100,000 km^2) over which winds are averaged in this study will likely smooth errors and accurately resemble the strength and direction of wind forcing in this region.

On average only 30% of daily ESACCI data over the shelf break is cloud-free. In order to improve Chl-a data coverage, data sets were averaged into 5-day composites (from daily for ESACCI, and hourly for ERA5), where the data at time t is the 5-day preceding mean (omitting cloud pixels in the case of ESACCI). The result generates a time series with 5-day time steps from January 5th to December 31st (leap years have a 6-day preceding mean for the March 1st composite). Even when composited, images with high cloud cover were prone to individual pixels with unrealistically high Chl-a concentrations (>5 mg/m^3 at cloud margins), so images with less than 5% data availability over the OSB were treated as completely covered by clouds. Each 5-day composite image is on average 75% cloud-free over the shelf, significantly improving per-image data coverage when compared to daily data.

Single-sensor AVHRR sea surface temperature (SST) images for the study region were retrieved from 23 December 2020 to 2 February 2021 (corresponding to timing of an oceanographic mooring deployment) from the Australian Ocean Data Network. The data set blends all available day and nighttime SST observations from NOAA polar-orbiting satellites at a 0.02° × 0.02° resolution (approximately 2 km at 45°S) into a daily SST image (Paltoglou et al., 2010). Each image was filtered to only include observations with "acceptable" quality or higher.

2.1.2. In Situ Data

In situ Chl-a, nitrate, salinity, and temperature measurements are from the Munida Transect time series, an ongoing long-term (1998–2021) bi-monthly-sampled transect off the Otago Peninsula (cyan line, Figure 1) (Currie et al., 2011). Chl-a and nitrate measurements were collected from the upper 10 m at 9 stations along the 60 km transect (approximately every 7 km on average), although not for all cruises ($n = 87$, $n = 20$, for Chl-a and nitrate, respectively). Chl-a analysis was performed following the filtration, preparation, and fluorometer methodology outlined in Jones et al. (2013). Nitrate samples were similarly processed following the filtration, preparation, and auto analyzer/segmented flow analyzer methodology described by Currie et al. (2011). Discrete Chl-a and nutrient sampling along the transect was complimented by continuous underway temperature and salinity measurements, providing high resolution surface temperature and salinity data for the whole transect length (Jones et al., 2013).

An ocean mooring deployment along the Munida Transect (140 m water depth, 45.823S 170.937E) collected water column temperature over 41 days during the summer period of 23 December 2020 to 2 February 2021. Temperature loggers were fitted at 0, 5, 10, 15, 20, 40, 60, 120, and 140 m depths, logging at either 1 s (upper 20 m), or 5 min intervals (below 20 m). For this analysis all temperature series were averaged to 5 min. A pressure logger at 0 m was also attached to discern periods of mooring blowdown. When the float was subsurface, effective logger depth was calculated assuming a straight mooring line between the float depth and fixed anchor depth of 140 m. Though a low-drag surface float was used, at times the mooring float was submerged over 50 m below surface.

Bathymetry data is from National Institute for Water and Atmospheric Research's (NIWA) 2016 New Zealand Regional model. The data set compiles bathymetry data from multi-beam and single beam surveys, digitized bathymetric charts, soundings, and navy collector sheets (Mitchell et al., 2012). In this study the original 250 m × 250 m gridded data was unprojected to latitude and longitude coordinates in order to match the coordinate systems of the remotely-sensed and in situ data.

2.2. Methods

2.2.1. Climatologies and Transects

Remotely-sensed median climatologies were produced at a 5-day resolution through calculating per-pixel medians for each 5-day block of the year, and smoothing with a moving mean window including two time steps before and after (±10 days). ESACCI Chl-a anomalies are generated by removing this climatology from the 5-day dataset.

Four Chl-a transect series were extracted from ESACCI fields within 30 × 90 km boxes rotated to be perpendicular to the shelf break (Figure 1). To improve data availability compared to a single line of points along the transect, the 30 km box height blends data parallel to the front. Mean Chl-a values are taken in 4 km increments along the 90 km transect length (to match ESACCI's spatial resolution), generating a spatially smoothed (approximately 6 pixels per 4 km increment) transect series from the 5-day composite time series. These transects are similarly fitted with 5-day median climatologies as outlined above. A Chl-a anomaly time series is generated for each transect by removing this median climatology from the 5-day data set.

2.2.2. Bloom and Wind Events

To identify anomalous Chl-a events along the OSB, a mean OSB Chl-a anomaly time series was calculated from the mean Chl-a anomaly between the 200 and 1,000 m isobaths across the entire OSB region. "Enhancement" events were identified as periods where mean OSB Chl-a anomalies exceeded 0.23 mg/m^3 (90th percentile of November–March Chl-a anomalies). "Reduction" events similarly were periods where mean OSB Chl-a anomalies were below −0.13 mg/m^3 (10th percentile of November–March anomalies). This approach is modified from other threshold-based Chl-a metrics (Oliver et al., 2022; Siegel et al., 2002) to instead consider anomalous values at the shelf break, as this study is primarily concerned with episodic enhancements/reductions and not the timing of seasonal blooms exceeding a concentration threshold. Consecutive 5-day composites with anomalies exceeding the aforementioned enhancement/reduction thresholds were considered singular "events." If two enhancement or two reduction events were only separated by one 5-day step, they were considered the same event. This approach accurately identified the onset of anomalous shelf break Chl-a concentrations (presented in Section 3.2).

Wind stress was rotated by 50° (average angle of the OSB) to obtain the along-front component. Significant AFW forcing was deemed to occur when 5-day averaged AFW stress magnitude exceeded 0.04 N/m^2 (70th percentile). Of all summer 5-day periods, 43 met the upfront threshold (≤ -0.04 N/m^2) and 165 downfront (≥ 0.04 N/m^2). Similarly, weak/strong wind stress forcing was deemed to occur when 5-day mean wind stress magnitudes were less than 0.03 N/m^2 (25th percentile)/greater than 0.08 N/m^2 (75th percentile), matching 173 summer periods for each. These stress thresholds make the upfront, downfront, and weak stress periods mutually exclusive, but there is overlap between upfront/downfront winds and strong stress periods. These wind thresholds were used for generating composite images of median Chl-a anomalies. Confidence intervals for composite medians are generated through bootstrapping the per-pixel median for 1,000 resamples (with replacement) of all summer Chl-a anomalies (Davison & Hinkley, 1997).

The methodology for identifying wind patterns preceding Munida Transect cruises had to be adjusted to account for a bias toward less intense wind stress days (mean wind stress magnitude of 0.037 N/m^2 on summer cruise days vs. overall summer mean of 0.054 N/m^2), as well as reduced data availability (51 summer cruises total). As such, any 5-day averaged AFW stress of <-0.01 N/m^2 was considered upfront, and 5-day averaged AFW stress >0.01 N/m^2 was considered downfront. Following the application of these criteria, there were 19 summer cruises following upfront events, and 17 summer cruises following downfront events.

3. Results

3.1. Remotely-Sensed Climatologies

Climatologies of Chl-a and wind forcing were established to quantify seasonal patterns and variability. Median 5-day climatologies along the broader OSB show relative shelf enhancement of Chl-a (inshore of the 200 m isobath) for the light-available summer months of November through to the end of March (Figure 3). Median summer Chl-a concentrations increase northward from transects a through d, generally highest over the shelf inshore of the 200 m isobath. During winter months median off-shelf Chl-a concentrations reach minimums of

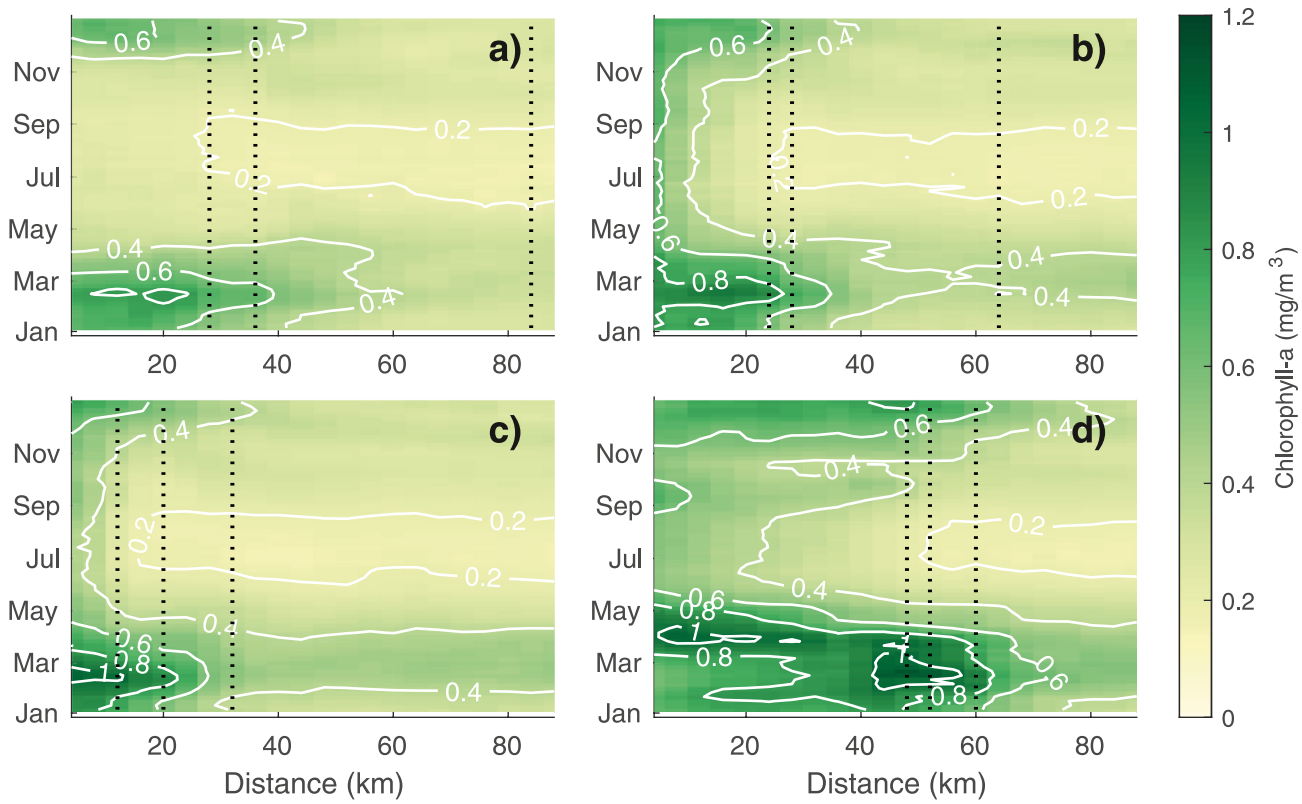

Figure 3. Median 5-day composite chlorophyll-a climatologies for transects a through d. White contours are spaced every 0.2 mg/m^3, dashed lines indicate the 200, 500, and 1,000 m isobaths (moving left to right off-shelf).

<0.2 mg/m^3 in all transects. The largest seasonal range in Chl-a occurs in transect d between July and February, changing 0.93 mg/m^3 at the shelf break. Peak Chl-a along transect d occurs at the shelf break from January to March, shifting inward over the shelf in late March. For all other transects, peak seasonal chlorophyll occurred at or inshore of the 200 m isobath, with no clear seasonal shelf break bloom.

Median Chl-a concentrations along the OSB are highest at the shelf break surrounding Te Pātaka o Rākaihautū/Banks Peninsula during the Austral Summer (November–March) (Figure 4a). South of this region, median surface Chl-a over the entire shelf is elevated during the summer, especially relative to off-shelf SAW to the east. To the west of the Snares Plateau, Chl-a concentrations exceeding 0.4 mg/m^3 are found off-shelf, corresponding to the general position of the subtropical front before it is steered along the OSB (Chiswell et al., 2013). Patterns in summer Chl-a variability mostly reflect patterns in median Chl-a, although variability is particularly constrained to the shelf break north of the Otago Peninsula (Figure 4b). Variability is relatively low over the shelf, with values comparable to those in SAW further offshore.

Median summer wind stress over southern ANZ was most intense over the Snares Plateau, with reduced stress off the east coast on the leeward side of ANZ (Figure 5a). Strong westerlies characteristic of the Southern Ocean were not prevalent at the OSB, where winds were predominantly shelf break aligned as a consequence of orographic steering around the ANZ landmass (Kidson, 2000; Sturman et al., 1984). Regular summer oscillations between up and downfront winds along the OSB meant that median wind vectors in the southern OSB were small and slightly off-shelf, becoming increasingly upfront to the north.

Summer winds over the OSB were generally weaker and the most shelf break aligned (Figure 5b), with 65% of winds occurring within 40 degrees of the shelf break and a median speed of 4.6 m/s. The along front component of summer winds was more often upfront (negative 53% of the time) than downfront (positive 47% of the time). However, as downfront wind stress periods were generally more intense, mean AFW speed is slightly positive (0.1 m/s). Winds during other seasons are both stronger and less shelf break aligned, with the winter months (Figure 5d) being the most westerly, with a median speed of 5.8 m/s.

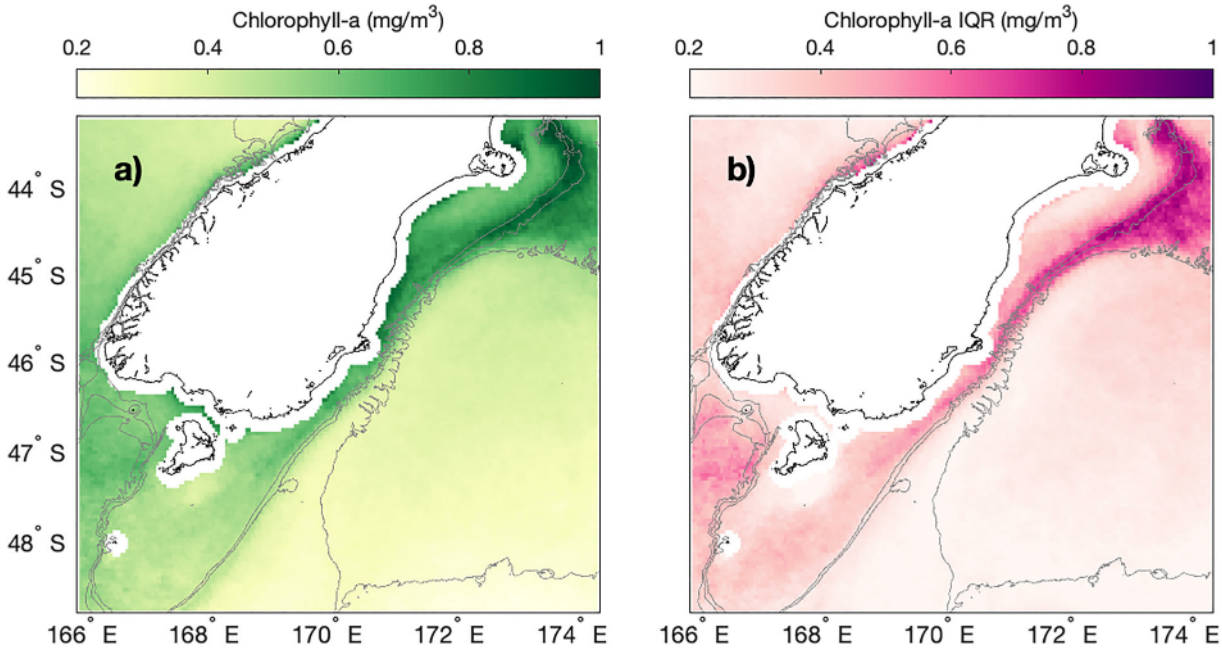

Figure 4. Median summer (November–March, inclusive) chlorophyll-a concentrations (a). Summer chlorophyll-a interquartile range (b). The 200, 500, 1,000 m isobaths are outlined in gray. Values within 15 km of the coast are masked.

3.2. Remotely-Sensed Images and Wind Forcing

In order to understand the conditions preceding anomalous Chl-a at the OSB, anomalously high "enhancement" and anomalously low "reduction" Chl-a periods were identified. Wind conditions prior to the onset of these periods were evaluated to identify wind forcing potentially associated with enhancement or reduction of Chl-a at the OSB. Cursory inspection of the OSB Chl-a anomaly time series appeared to show a relationship between enhancement onset (red stars) and negative (upfront) AFW stress (Figure 6a). Compositing AFW stress prior to

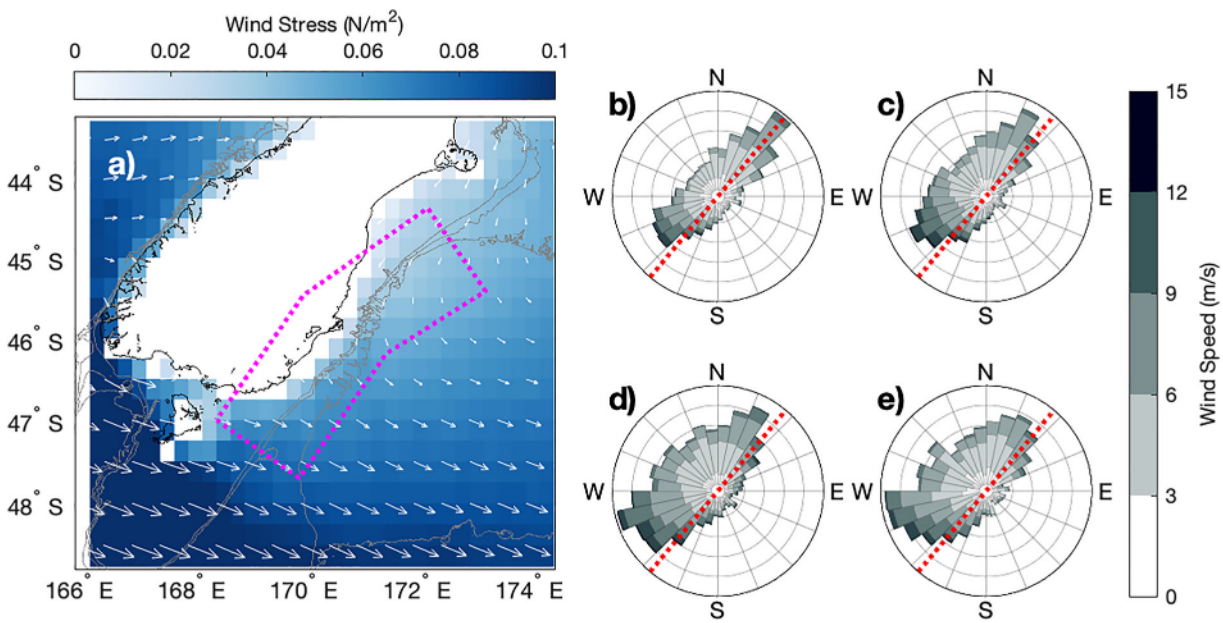

Figure 5. Median summer (November–March) wind stress (a). Magenta box indicates Otago Shelf Break (OSB) area over which winds were averaged, white arrows show median wind direction. Seasonal wind speed and direction distributions for summer, autumn, winter, and spring (b through e, respectively). Red line indicates average angle of the OSB.

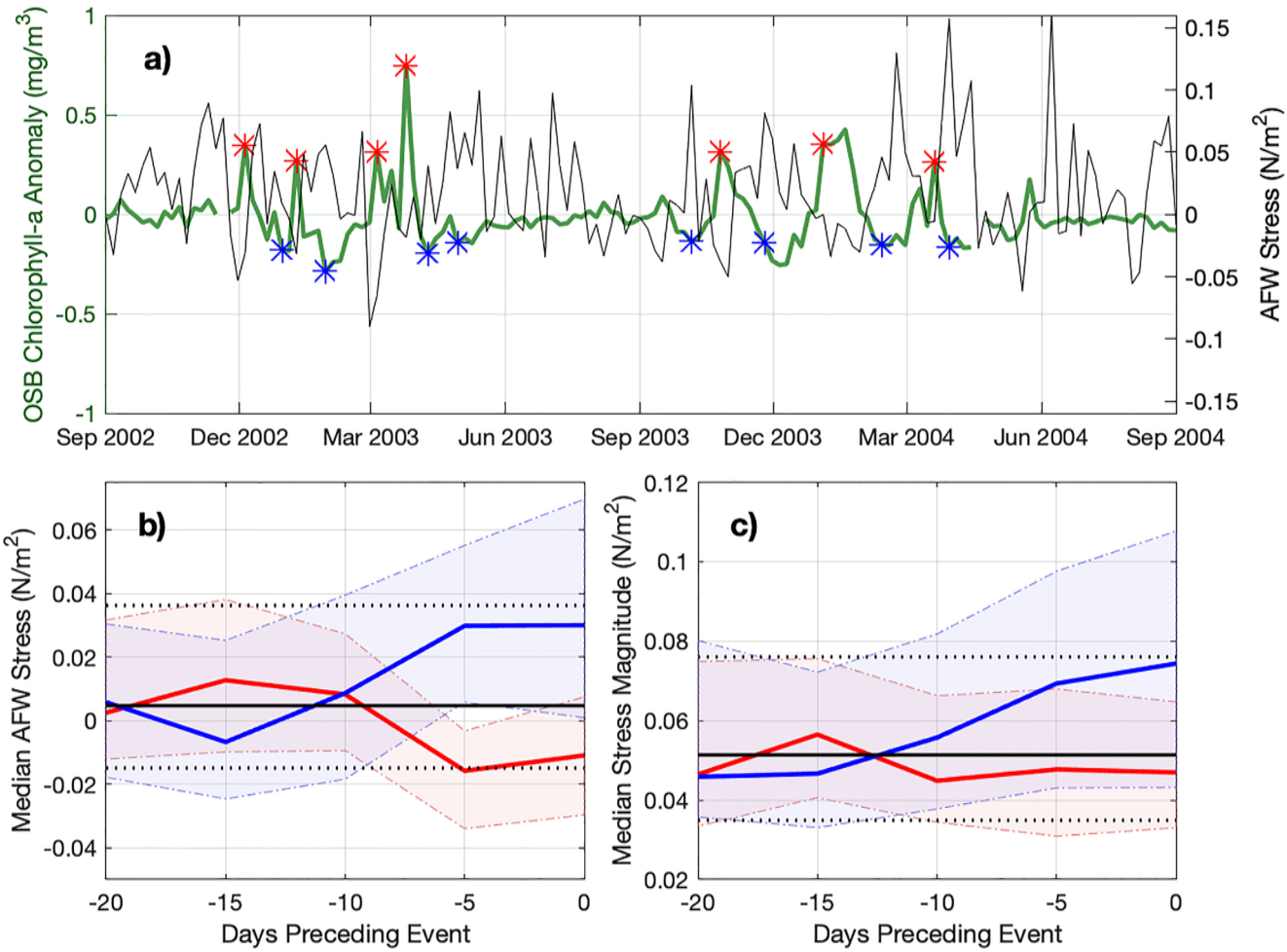

Figure 6. Two-year subset of 22-year median Otago Shelf Break (OSB) chlorophyll-a anomaly time series (green curve), and OSB along-front wind (AFW) stress anomaly (gray curve) (a). Red stars indicate days of enhancement onset, blue indicate days of reduction onset. Median AFW stress in the 15 days preceding enhancement (red) and reduction (blue) events (b). Median wind stress magnitude in the 20 days preceding enhancement (red) and reduction (blue) events (c). Shaded areas indicate interquartile range. Solid black lines in (b) and (c) indicate median value, dashed black lines indicate interquartile range.

enhancement and reduction events revealed that winds were more frequently upfront preceding Chl-a enhancement events ($n = 69$), and more frequently downfront preceding Chl-a reduction events ($n = 57$) (Figure 6b). The difference in median AFW forcing began in the period 10 days prior and was most pronounced in the period 5 days before the event. Using Mood's median test, the differences between median AFW stress preceding enhancement and reduction events were significant ($p < 0.01$) at 5 and 0 days lag, and not significant at 95% confidence for other periods. When repeating this analysis in terms of wind stress magnitude, there was no significant pattern preceding Chl-a enhancement events, whereas Chl-a reduction events were associated with intensified wind stress, beginning in the period 10 days before and most significant at a 0-day lag ($p = 0.049$) (Figure 6c).

OSB enhancement events were generally short-lived, with 72% of events persisting for 10 days or less (Figure 7a), consistent with the episodic nature seen in daily remotely-sensed images (Figure 2). Events began in the Austral Summer (November–March) 77% of the time (Figure 7b), with peak mean OSB Chl-a values of around 0.8 mg/m^3 (Figure 7c). Chl-a reduction events were overall more long-lived than Chl-a enhancement events, with 45% of events remaining between 10 and 20 days (Figure 7e). Similarly, 65% of reduction events occurred in the Austral Summer (Figure 7f). Reduced Chl-a values were marked by OSB concentrations of around 0.28 mg/m^3 (Figure 7g). The occurrence of these events highlights significant sub-monthly Chl-a variability at the OSB during light-available months.

Following the lagged Chl-a response to AFW suggested in the previous analysis, linear correlations between AFW stress and 5-day lagged OSB Chl-a anomaly were computed ($R = -0.37$, $p < 0.01$, not pictured). To

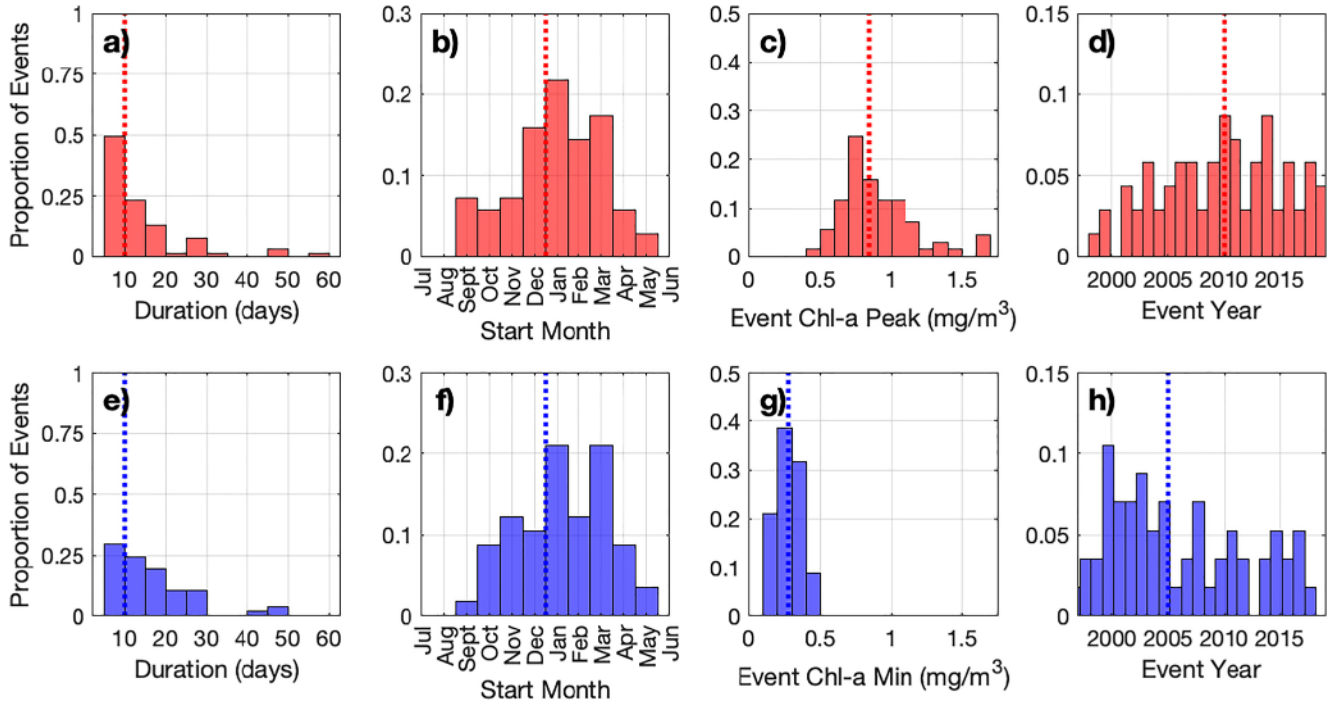

Figure 7. Duration, start month, peak/minimum Chl-a, and year of occurrence distributions for enhancement events ($n = 69$, red) and reduction events ($n = 57$, blue). Vertical lines indicate median values.

better visualize this relationship, OSB Chl-a anomalies were binned in terms of the mean AFW stress 5 days prior (Figure 8). The lack of overlap between box plot notches (McGill et al., 1978) shows there was a significant difference (0.29 mg/m^3, $p < 0.05$) in median OSB Chl-a anomaly between strong upfront wind stress (<−0.04 N/m^2) and strong downfront wind stress (>0.04 N/m^2) (Figure 8a). The difference was less pronounced (0.1 mg/m^3) between medium-light upfront and downfront wind stress, although still significant ($p < 0.05$).

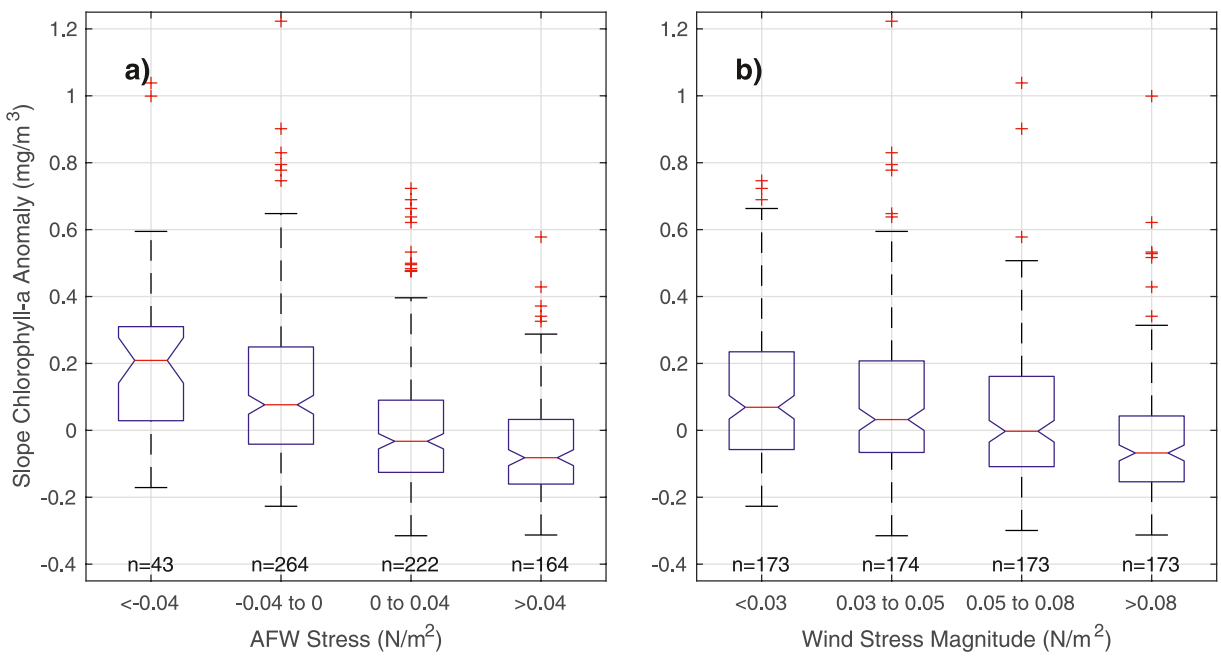

Figure 8. Slope chlorophyll-a anomaly distributions for binned along-front wind stress (a), and binned wind stress magnitude (b).

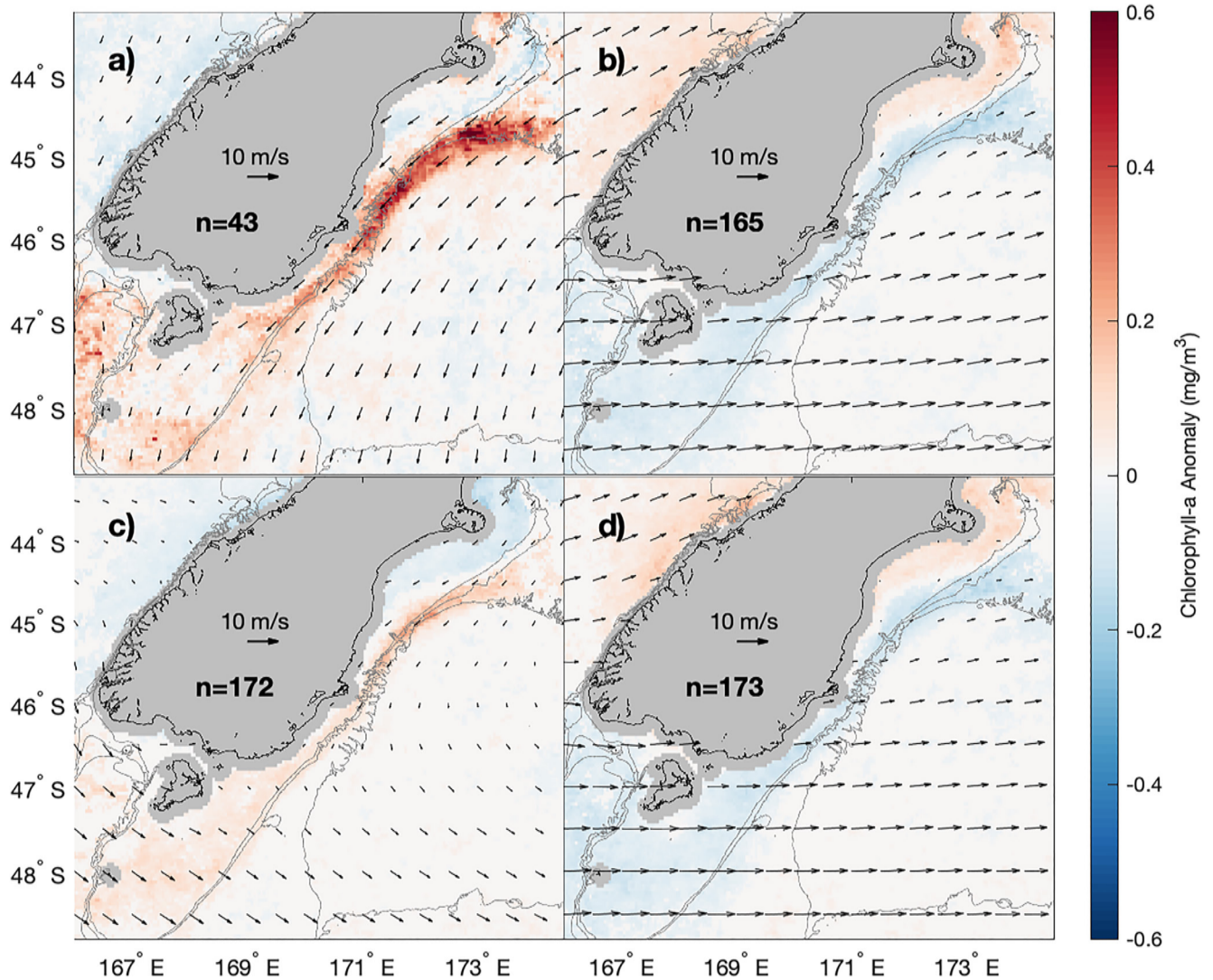

Figure 9. Median 5-day lagged chlorophyll-a anomaly composites for significant upfront wind stress (a), significant downfront wind stress (b), anomalously weak wind stress (c), and anomalously strong wind stress (d). Areas not significantly different from 0 at 99% confidence intervals were masked as 0. Black vectors show median wind speeds (every other vector from ERA5 plotted for clarity), gray contours show 200, 500, and 1,000 m isobaths.

As found with Figure 6, the relationship between summer OSB Chl-a anomalies and wind stress magnitude was less pronounced than for AFW stress ($R = -0.22$, $p < 0.01$, not pictured). Chl-a anomalies binned by preceding wind stress magnitude had no significant median difference for stress less than 0.08 N/m^2, although high wind stress (>0.08 N/m^2) was generally followed by negative Chl-a anomalies (median anomaly of −0.07 mg/m^3) (Figure 8b). High wind stress periods largely consist of downfront winds (86% of events in this bin), hence the resemblance to Chl-a anomaly distribution seen following strong downfront winds in Figure 8a.

Spatial composites of 5-day lagged Chl-a anomalies as a function of wind stress show a pronounced enhancement of Chl-a along most of the OSB following significant upfront wind stress, beginning where the shelf narrows and deflecting toward the Chatham Rise (Figure 9a). There was a similar Chl-a decrease along the OSB following significant downfront stress, although this was smaller in magnitude (Figure 9b). A small but significant positive Chl-a anomaly over the shelf around Banks Peninsula is apparent following downfront stress, potentially indicating movement of Chl-a concentrations toward the coast. North of the Otago Peninsula the median Chl-a anomaly difference between upfront and downfront wind stress exceeded 0.8 mg/m^3 over the shelf break, a difference comparable to the seasonal cycle at this part of the OSB (0.9 mg/m^3). Weak wind stress was associated with an enhancement along the OSB (Figure 9c), but this was located further inshore, narrower, and less intense than

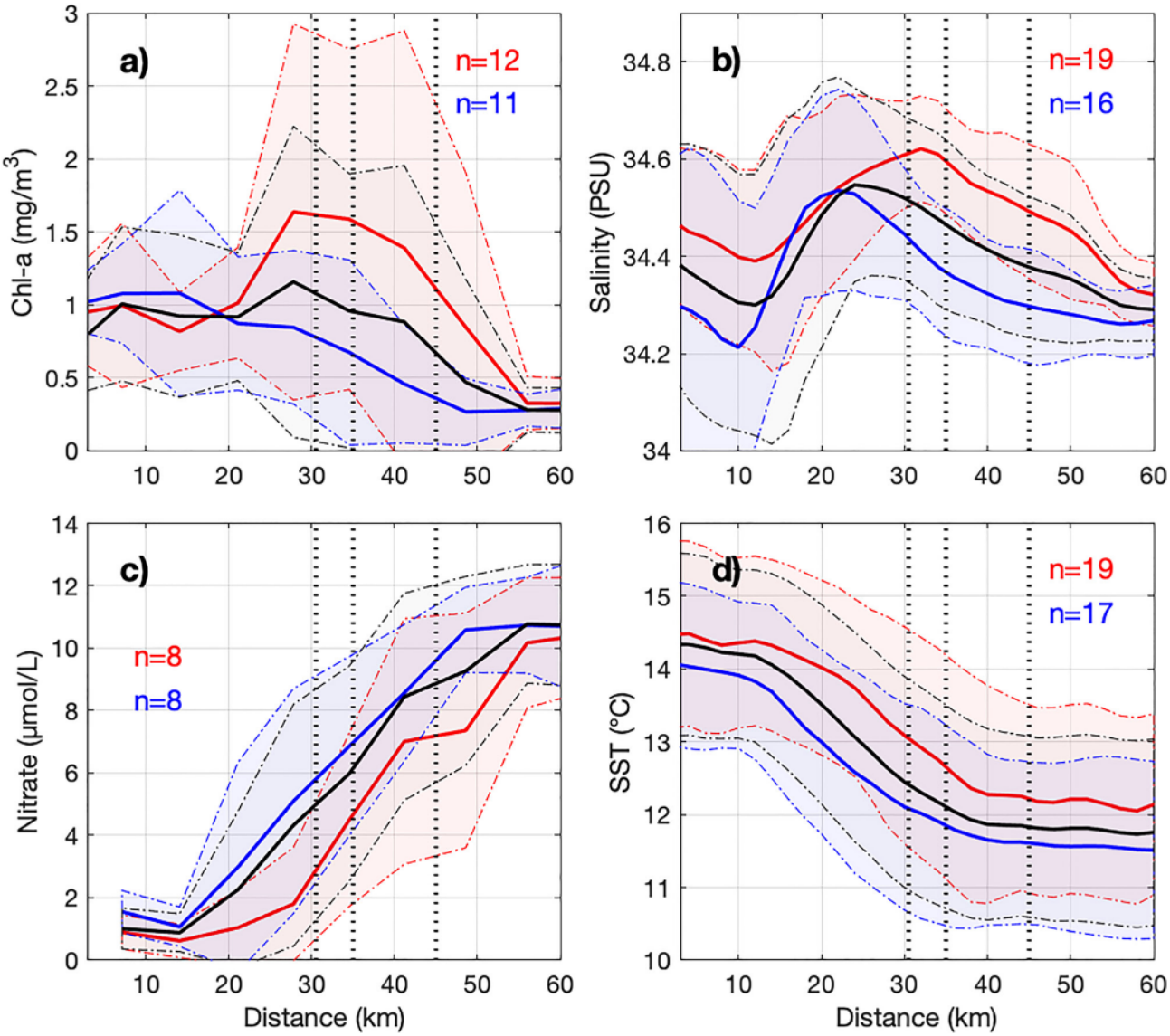

Figure 10. Munida Transect chlorophyll-a (a), salinity (b), nitrate (c) and temperature (d). Transects were binned by along-front wind stress in the preceding 5 days, with red indicating upfront, blue indicating downfront, and black showing all summer transects. Solid lines indicate medians, shaded areas indicate the interquartile range. Dashed vertical lines indicate 200, 500, and 1,000 m isobaths (left to right).

following strong upfront wind stress (anomaly composite peak 0.29 mg/m^3, vs. 0.88 mg/m^3). The composite of anomalously strong wind stress magnitude (Figure 9d) displayed a similar pattern to that of significant down-front stress, as 80% of these events overlap. Similar patterns were visible in composites at 0 lag, but they were significantly weaker for all composites (not shown), suggesting that the Chl-a response to wind stress is lagged by approximately 5 days.

3.3. In Situ Measurements and Wind Forcing

To further build on remotely-sensed Chl-a findings and offer insight into physical properties such as salinity, temperature, and nitrate, historic in situ Munida Transect data were composited by mean AFW stress in the prior 5 days. Summertime surface Chl-a along the transect was enhanced following upfront wind stress ($n = 12$), consistent with patterns observed from remotely-sensed data (Figure 10a). This increase in Chl-a was pronounced beyond the 200 m isobath, past the average summer position of the shelf break front, which lies approximately over the 200 m isobath along this transect (Hopkins et al., 2010). Downfront wind stress ($n = 11$) was followed

by significantly smaller surface Chl-a concentrations at the shelf break, with peak values generally occurring in the innermost stations less than 20 km from the coast.

Surface salinity following upfront periods ($n = 19$) showed a widening of the high salinity band associated with STW at the shelf break front (Figure 10b). Following downfront wind stress ($n = 16$), median surface salinity showed a narrower salinity peak and relatively reduced surface salinity overall. Waters with salinity less than 34.5 PSU and temperatures below 12°C, generally considered SAW, were present offshore of the 1,000 m isobath following upfront winds, and inshore of the 200 m isobath following downfront winds, suggesting an offshore/onshore movement of the surface expression of the front following upfront/downfront wind stress.

Surface nitrate concentrations (Figure 10c) were reduced following upfront wind stress ($n = 8$) relative to downfront wind stress ($n = 8$). This is pronounced beyond 15 km along the transect, over the outer shelf and shelf break. Mean surface nitrate concentrations are below 1 μmol/L over most of the shelf following upfront wind stress, increasing beyond the 200 m isobath.

Surface temperatures were elevated following periods of upfront stress ($n = 19$) relative to those following downfront winds ($n = 17$) (Figure 10d). Warmer shelf waters extend further along the transect following upfront winds, with the steepest cross-shelf gradient occurring 26 km offshore. Following downfront winds, peak temperature gradients occur nearer to the coast, at 16 km along the transect. Temperature ranges across the front are similar in magnitude between upfront and downfront winds, dropping approximately 2°C between shelf and off-shelf waters.

Moored temperature data from December–February in the Austral summer of 2020/2021 allowed insight into the evolution of water column structure in response to AFW stress. Figure 11 shows a relatively cloud-free example of a shift from downfront to upfront winds, a transition which occurred six times through the deployment (approximately every 8 days). This wind reversal was associated with a transition from a well-mixed water column on December 27th (surface-bottom temperature difference, ΔT, of <1°C) to one that is highly thermally stratified ($\Delta T > 4$°C) on the 29th of December. At the beginning of this transition, the thermal structure was well-mixed, although periods of mooring blowdown masked the upper 50 m at times, and the shelf break was near median Chl-a concentration (Figure 11d, leftmost frame). Warmer shelf waters appeared to be constrained nearshore, with cool waters (<12°C) over the shelf break (Figure 11c, leftmost frame). As the AFW stress slackened and shifted upfront on December 27th, the mooring float returned to the surface and revealed a well-mixed water column. Upfront wind stress continued to increase in intensity, and thermal stratification began to develop (from $\Delta T < 1$°C to $\Delta T > 4$°C between December 28th and 29th), coinciding with the appearance of significant positive shelf break Chl-a anomalies from December 29th onward. SST images show that warm shelf waters moved over the shelf break during this time, with temperatures >12°C reaching the 1,000 m isobath. Following this period the upfront wind stress weakened, but remained upfront, and thermal stratification remained from December 30th through to January 1st. High Chl-a values are visible on the 31st of December despite cloud cover, suggesting that the bloom continued to intensify. Unfortunately, high cloud cover remained for the subsequent week, so the conditions over the complete duration of the bloom event could not be analyzed. Daily (non-anomaly) Chl-a images indicate that the bloom increases in intensity while moving offshore, rather than simply advecting high Chl-a to the shelf break (Figure 11e).

4. Discussion

4.1. Chlorophyll-a Patterns at the OSB

This study sought to identify and characterize episodic Chl-a blooms along the OSB and test their relationship to AFW forcing. Shelf break climatologies showed yearly Chl-a maxima in summer just above 1 mg/m^3, comparable in magnitude to the seasonality observed over the Chatham Rise (Chiswell et al., 2013), but with peak intensity occurring later from January–March versus November–December. The timing of elevated Chl-a from ESACCI climatologies (Figure 3) was in better agreement with occurrence of summer blooms noted by Jones et al. (2013), although evidence of spring blooms observed in their work is absent from transect climatologies presented in this study.

OSB blooms represent significant episodic increases in local Chl-a, comparable to the magnitude of the seasonal cycle for the region. This has potentially important implications for the ecology of southern ANZ marine species,

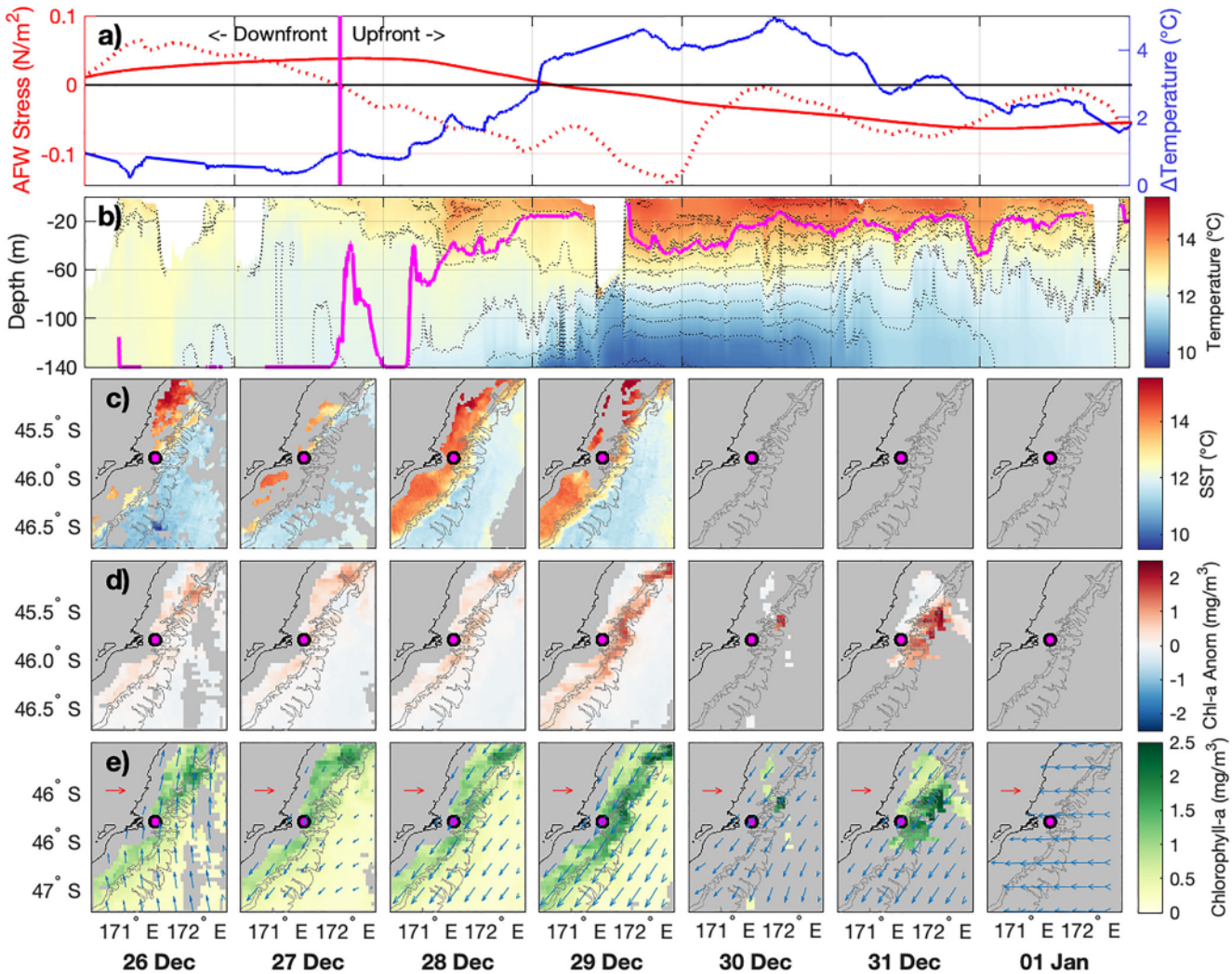

Figure 11. Along-front wind (AFW) stress (red) and mooring surface-bottom temperature difference (blue), (a). Dashed red line is daily AFW stress, smooth red line is 5-day preceding running mean. Magenta line indicates time when wind shifts from downfront to upfront. Water column temperature from in situ mooring, (b). Solid black contours space 1° isotherms, dashed contours 0.5°, magenta contour shows mixed layer depth (defined as 0.8°C change from surface). 24-hr AVHRR sea surface temperature composite, (c). Daily ESACCI chlorophyll-a anomaly, (d). Daily ESACCI chlorophyll-a, (e). Mooring position indicated by magenta dot, and 200, 500, 1,000 m isobaths are contoured in gray. Blue vectors in row (e) show daily wind velocity, red arrow indicates 5 m/s scale.

as previous work has linked increased species richness from trawling catch data to the heightened productivity and temperature gradients observed along the OSB (Leathwick et al., 2006). During large shelf break blooms, such as that pictured in Figure 2, surface Chl-a concentrations tripled over a 350 km section of the shelf break, representing the highest surface Chl-a values for that year. Connections between summer bloom events and AFW variability (Sections 3.2–3.3) highlight the need for understanding future climatic changes that may affect the direction and strength of AFW forcing. For example, if there is an increase in the occurrence of northeasterly weather systems across ANZ as a result of climate change (Bodeker et al., 2022), more frequent upfront wind forcing may lead to an increase in the number of episodic bloom events at the shelf break.

Large-scale climate oscillations, such as the El Niño Southern Oscillation (ENSO), have been connected to variations in front gradients (Hopkins et al., 2010), and southwesterly strength (Kidson, 2000) over the OSB, potentially driving interannual variability in surface Chl-a. Stronger southwesterlies, associated with El Niño conditions (Kidson, 2000), may contribute to the relatively more frequent Chl-a reduction events at the OSB from 2000 to 2005, years generally associated with positive ENSO. Weakening of frontal temperature gradients at the OSB, also associated with El Niño conditions (Hopkins et al., 2010), may reduce the magnitude of Ekman-induced buoyancy fluxes, weakening the isopycnal response upfront/downfront wind stress. However, the strong El Niño

conditions observed through 2015 (Figure S2 in Supporting Information S1) did not result in an apparent change in the frequency of OSB Chl-a reductions/enhancements, prompting the need for more focused analysis of factors underpinning interannual variability of OSB bloom events.

Despite the locally high surface concentrations of Chl-a over the OSB, the magnitude of Chl-a observed was low compared to shelf break systems on a global scale (Carranza et al., 2017; Oliver et al., 2022; Xu et al., 2011), agreeing with previous observations in the region (Boyd et al., 2004; Jones et al., 2013). Individual 5-day composite images very rarely had concentrations exceeding 4 mg/m^3 anywhere along the OSB through the entire record. This contrasts strongly with the Patagonia system whose mean summer concentrations are near or exceeding 4 mg/m^3 along the entire shelf break (Carranza et al., 2017).

4.2. Position and Timing of OSB Enhancement

Surface enhancement of Chl-a during summer at the OSB is generally preceded by upfront wind stress (Figures 6b and 8a). This is in contrast with the pattern observed at the Patagonian Shelf Break by Carranza et al. (2017) who found the greatest Chl-a enhancement following downfront winds. Composites following downfront AFW stress along the OSB (Figure 9b) only show slight enhancement (<0.2 mg/m^3) over the shelf immediately south of Banks Peninsula (44°S), unlike the comparatively intense enhancement (>0.5 mg/m^3) observed in the Patagonian system inshore of the shelf break (Carranza et al., 2017). North of the Otago Peninsula median Chl-a concentrations clearly shift offshore following upfront wind stress (Figures 9a and 10a), whereas Chl-a concentrations following upfront wind stress in the Patagonian system showed no significant movement relative to mean conditions. Density profiles from hydrographic transects show that peak Chl-a at the Patagonian shelf break occurs shoreward of dense off-shelf waters, consistent with elevated surface Chl-a observed inshore of SAW off of the Otago Peninsula (Figures 10a–10c). Thus, though blooms in each study appear to occur in similar locations relative to frontal position, the response to AFW stress differs, with the most-significant Chl-a enhancement occurring at each system in response to differing directions of AFW. This suggests that different physical mechanisms and/or phytoplankton limitations are involved.

From the data used in the current study, it is challenging to evaluate what role nutrient enhancements play in the Chl-a response to AFW stress observed at the OSB. The shelf break nutrient pump model put forth by Siedlecki et al. (2011) relies on an oscillatory wind stress through which upfront winds first move slope waters onto the shelf, and subsequent downfront winds entrain this nutrient-rich slope water into the photic zone. In the winter, this numerical model generated enhanced primary productivity on the shelf side of the front following downfront wind stress, consistent with the patterns observed by Carranza et al. (2017) at the Patagonian shelf break. Siedlecki et al. (2011) also found that productivity increased in response to upfront wind during stratified summer conditions. This is out of phase with the largest vertical velocities over the shelf, which generate increased productivity due to nutrient entrainment in the winter model run. The authors attribute this seasonal change to a weakened nutrient pump during summer stratification, where upfront wind stress upwells nutrients to the surface at the shelf break front rather than drawing slope water onto the shelf (Siedlecki et al., 2011). Moored temperature observations at the OSB (Figure 11b) suggest that the Otago Shelf is well-mixed following downfront winds, with mixed layer depths at the seabed (140 m), unlike the stratification that persists through summer simulations in the Siedlecki et al. (2011) model. This would suggest that a more winter-like nutrient pump mechanism may be present at the OSB, which is consistent with observations of increased nitrate over the outer shelf and shelf break (Figure 10c). However, the OSB does not experience enhanced Chl-a following downfront winds as this model would predict, and there are no clear surface signs of upwelling at the OSB front from Munida Transect data (Figure 10) following upfront winds. As median nitrate concentrations are well above limiting concentrations over the shelf break (>3 μmol/L) (Eppley et al., 1969) during both downfront and upfront winds, it seems that other mechanisms are involved in explaining OSB Chl-a enhancement.

It is notable that nitrate profiles across the OSB (Figure 10c) differ significantly from the nutrient profiles used in the aforementioned numerical models (Franks & Walstad, 1997; Siedlecki et al., 2011; Whitt et al., 2017). In the OSB system, off-shelf SAW waters are abundant in macronutrients at the surface (Boyd et al., 1999; Currie et al., 2011; Jones et al., 2013), where the main limiting factors are nutrients such as iron, and silicate (in the case of diatoms) (Boyd et al., 1999, 2004; Jones et al., 2013). This is in contrast with the depth-dependent nutrient profiles used in the aforementioned numerical models, which have no initial lateral gradients. When nitrate or iron are at limiting concentrations, surface Chl-a at the OSB front could be enhanced through increased

cross-frontal mixing, alleviating macronutrient limitations in STW and iron/silicate limitations in SAW (Boyd et al., 2004; Chiswell et al., 2013; Jones et al., 2013). Entrainment of nutrients drawn onto the shelf as outlined by Siedlecki et al. (2011) is thus not strictly necessary to generate increases in Chl-a at the OSB, provided cross-shelf exchange is also likely to occur (Boyd et al., 2004). Following upfront winds, there appears to be a widening of the transitional zone between warm, salty waters associated with STW, and cool, relatively fresh off-shelf SAW (Figures 10b and 10d). The widening of the frontal region potentially corresponds to a greater area of mixing and nutrient exchange across the front (Boyd et al., 2004), although similarly to the Siedlecki et al. (2011) model, the absence of increased Chl-a in the narrow frontal region during downfront winds suggests that cross-frontal mixing does not fully explain the observed episodic blooms.

The results in this study appear to be more consistent with those of Oliver et al. (2022), who observed Chl-a enhancement at the Mid-Atlantic Bight shelf break front following upfront wind forcing. These Chl-a enhancements occur in spring following upfront winds due to Ekman restratification, alleviating light limitation in nutrient-replete waters. Salinity profiles indicate that peak Chl-a occurs in waters inshore of SAW (Figure 10), which are primarily nitrate limited (Boyd et al., 1999, 2004; Chiswell et al., 2013; Jones et al., 2013), and nitrate profiles at the OSB do not indicate limiting concentrations (median concentrations are >3 μmol/L) during either upfront or downfront winds (Figure 10c). Thus, considering the deep mixed layers observed following downfront winds at the outer shelf (Figure 11b), it is plausible that the OSB episodically resembles the nutrient-replete and light limited conditions described in Oliver et al. (2022) in summer months.

Unlike the Mid-Atlantic Bight, spring blooms following upfront wind stress are not as frequent at the OSB, occurring more prominently in summer (Figure 7b), though the latitudes of each region are comparable (47°–43°S for the OSB, 38°–42°N for Mid-Atlantic Bight). Significant OSB blooms occur regularly in February and March (late-summer/early autumn) but not as frequently in October and November (late-spring/early summer), months where photosynthetically active radiation is comparable (Chiswell et al., 2013), potentially pointing to differences in the hydrographic conditions that allow for Ekman restratification. This difference may be due to the relatively weak temperature gradients of the OSB front in spring (Hopkins et al., 2010), in comparison to the Mid-Atlantic Bight which sees its strongest density gradients in winter and spring (Oliver et al., 2022). This would generate less pronounced vertical stratification following offshore Ekman transport along the OSB in spring, minimizing the increase in water column stability from slumping isopycnals. An additional factor could be due to less frequent upfront winds over the OSB during spring (Figure 5e), generating offshore Ekman transport less often.

4.3. Proposed Mechanism

The direction of AFW stress better predicts anomalous shelf break Chl-a concentrations than wind stress magnitude alone (Figure 8). The Chl-a reduction observed at the OSB following periods of strong wind stress (Figure 9d) indicates that surface Chl-a may be moved away from the surface by intense mixing, however, these events are largely associated with downfront winds (Figures 5b and 9d). If downfront winds are removed from the strong wind stress composite, the Chl-a anomaly is positive along the OSB (not pictured); suggesting the pattern observed following strong wind stress is more related to the large proportion of downfront wind events in that composite rather than the magnitude of wind stress alone. During weak winds a slight enhancement at the shelf break was observed (Figure 9c), suggesting that reduced wind stress does increase surface Chl-a, albeit not to the same degree as that associated with upfront forcing. As such, the factors driving observed Chl-a patterns are likely more dependent on how the wind direction and the associated Ekman circulation interact with the vertical structure of the OSB.

A plausible explanation for OSB enhancement following upfront wind stress is Ekman restratification at the shelf break front, outlined in a schematic (Figure 12) modelled after Siedlecki et al. (2011); Carranza et al. (2017); Oliver et al. (2022). This mechanism of episodic alleviation of light limitation in deep mixed layers at the shelf break is analogous to Ekman restratification in other mid-to-high latitude systems (Franks & Walstad, 1997; Hopkins et al., 2021; Long et al., 2012). It differs in that the well-mixed conditions at the shelf break are driven by episodic downfront wind events rather than seasonal patterns in shelf heating. Here, we propose that deep mixed layers and strong turbulent mixing follow downfront wind stress and create conditions similar to those in early spring (Hopkins et al., 2021; Zarubin et al., 2017). This mixes phytoplankton through the water column out of the photic zone, resulting in negative surface Chl-a anomalies (Figure 12a). Once winds turn upfront and Ekman restratification occurs at the shelf break, phytoplankton are able to accumulate in a shallow, stratified, illuminated

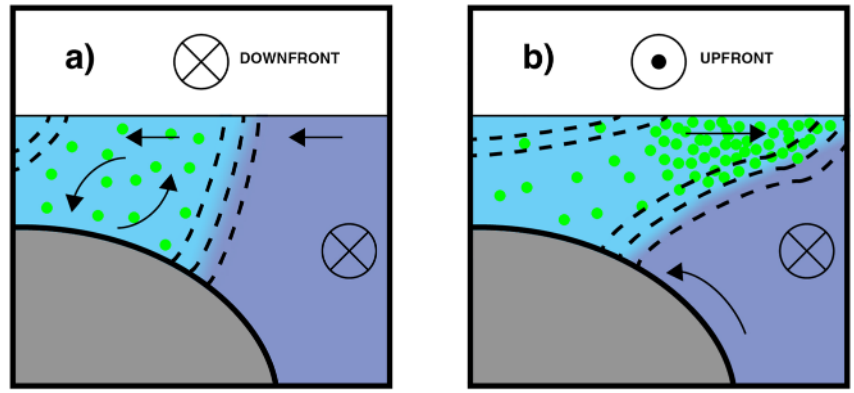

Figure 12. Proposed shelf break bloom mechanism at the Otago Shelf Break during downfront winds (a), and upfront winds (b). Dashed lines show isopycnal structure, arrows indicate general direction of water movement, green represents chlorophyll-a concentrations.

layer, episodically generating large summer Chl-a signals at the shelf break (Figure 12b). It is possible that the oscillation between these two regimes also allows nitrate to be replenished at the shelf break during downfront winds (Siedlecki et al., 2011), and the relatively short lived nature of upfront wind events means that phytoplankton cannot fully deplete nitrate concentrations at the shelf break before winds shift downfront and cease the episodic bloom event through deep mixing. This proposed mechanism would be expected to lead to blooms only around the shelf break front, where water depths and strong horizontal density gradients allow the water column to shift between deeply mixed (MLD > 200 m) and highly stratified (MLD < 40 m) in response to AFW stress.

The downfront mode of this schematic (Figure 12a) is supported by evidence of a well-mixed mid-shelf water column (Figure 11b), reduction of Chl-a concentrations over the shelf break (Figure 9b), and Chl-a maximums in shallow waters (Figure 10a) all following downfront winds. The upfront mode of this schematic (Figure 12b) is supported by evidence of offshore frontal adjustment (Figures 10 and 11c), stratification development over the mid shelf (Figure 11b), and a distinct shelf break response (Figure 9) after upfront winds. The 5-day lag between Chl-a anomalies and AFW stress is consistent with the Ekman spin-up time of a 50 m mixed layer at this latitude (approximately 5.7 days, following formula (6) from Siedlecki et al. (2011)). It is also notable that cross-shelf transects conducted by Jones et al. (2013) following a period of upfront winds in December 2009 showed a phytoplankton bloom with highly similar structure to that predicted by this model. Periods of significant upfront wind stress (<-0.04 N/m^2) that were not accompanied by shelf break Chl-a enhancement occurred predominantly in the austral winter (20% of such events occurring in July). This suggests that wintertime turbulent convection may inhibit Ekman restratification at the shelf break (Taylor & Ferrari, 2011), restricting this mechanism in winter months.

4.4. Limitations

It is important to note that this study exclusively utilizes surface Chl-a measurements. Subsurface Chl-a maxima are a regular feature of shelf break fronts, and elevated depth integrated Chl-a (and productivity, by proxy) does not always coincide with periods of high surface concentrations (Franks & Walstad, 1997). Thus, the relative Chl-a enhancements observed at the OSB following upfront winds may not correspond to the highest periods of depth-integrated Chl-a in this system. Investigation into the depth structure of Chl-a distributions and estimates of net primary productivity is needed to fully understand the relative change in productivity following these wind events. Similarly, this study only utilizes data from a single mooring for insight into the water column response to AFW stress. This deployment only spanned 2 months, and is limited by frequent periods of blowdown, creating gaps in the measurement of surface temperatures. Future work is required to better characterize the cross-shelf isopycnal response to AFW stress, and investigate the isopycnal structure outlined in the proposed schematic.

Through using 5-day composites, downfront advection of high Chl-a patches by the Southland Current are masked. Mean current velocities of approximately 20 cm/s (Chiswell, 1996) could advect Chl-a over 80 km downfront over the course of 5-days, which will be smoothed across the shelf break in composite images. Daily snapshots

of shelf break Chl-a seem to show a simultaneous, relatively uniform response across the shelf break (Figures 2 and 11e). Finer temporal-resolution Chl-a data, and/or Lagrangian particle simulations forced by upfront/downfront wind stress, would be required to adequately understand the spatial evolution of Chl-a patches and relevant response times along the OSB. Similarly, transient fine-scale features, such as submesocale eddies and frontal meanders, will be masked in the 5-day composites used in this study. Frontal meanders have been identified along the Southland Current, increasing in frequency north of the Otago Peninsula (Hopkins et al., 2010). These features can dramatically alter cross-shelf gradients, impacting stratification at the shelf break (Lévy et al., 2000; Xu et al., 2011). Little is known about the eddy regime in this region, although high-spatial resolution remotely sensed snapshots reveal submesoscale eddy-like features at the shelf break (e.g., Figure 2, 14th of December). Due to the density gradients present along the OSB, it is likely that submesoscale eddies occur along this front (Fox-Kemper et al., 2008; Mahadevan et al., 2012; du Plessis et al., 2017), and contribute to stratification and mixing. Mixed layer eddies may interact with AFW stress to intensify restratification during upfront winds (du Plessis et al., 2017), however further observations at fine temporal scales are required to quantify the impact of these features.

This study does not fully address whether downfront wind stress drives entrainment of nutrients over the shelf, or if there is upwelling at the shelf break front in response to upfront winds. Furthermore, the off-shelf movement of neritic-derived silicate following upfront wind stress (nearshore front depicted in Figure 12b) may be critical in driving diatom blooms at the SAW margin, as suggested by Jones et al. (2013). Future work analyzing the phytoplankton assemblages associated with these transient blooms, and corresponding cross-shelf silicate concentrations, would offer much greater insight into the nutrient regime following each event.

5. Conclusion

In both remotely-sensed and in situ Chl-a data, the occurrence of transient summer Chl-a enhancement at the OSB is linked to upfront wind stress. These events are largely summer phenomena, and lag upfront wind stress at roughly 5-day time scales, consistent with Ekman spin-up time. Ekman restratification is proposed as a plausible mechanism facilitating the blooms observed at the front, supported by observations of nutrient-replete conditions at the shelf break, on/offshore frontal movement, deepening/shoaling of the outer shelf mixed layer, and a distinct shelf break response following downfront/upfront wind stress. When winds are downfront, we suggest that onshore Ekman transport generates vertical isopycnals and deep mixed layers at the shelf break, resulting in spring-like conditions associated with negative surface Chl-a anomalies. Through flattening isopycnals at the shelf break front in response to upfront winds, we propose that Ekman restratification creates a stable stratified layer, increasing access to light and allowing greater drawdown of nutrients. This mechanism possibly supports OSB blooms as large as the seasonal cycle, with potentially significant implications for the marine ecosystem of southern ANZ. Further insight into current velocities and water column structure at the OSB are needed to evaluate the role of nutrient transport and the relationship between observed surface patterns, water column structure, and depth-integrated productivity.

Data Availability Statement

ESACCI ocean colour data is available from: https://www.oceancolour.org/thredds/catalog-cci.html?dataset=CCI_ALL-v5.0-1km-DAILY (Sathyendranath et al., 2021). ERA5 wind data is available from: https://cds.climate.copernicus.eu/cdsapp#!/dataset/reanalysis-era5-single-levels (Hersbach et al., 2023). AVHRR SST is available from: https://portal.aodn.org.au/search (IMOS, 2022) IMOS is supported by the Australian Government through the National Collaborative Research Infrastructure Strategy and the Super Science Initiative. NIWA bathymetry data is available from: https://data-niwa.opendata.arcgis.com/datasets/nz-bathymetry-250m-imagery-raster-layer/explore (Mitchell et al., 2012). All in situ data is available from: https://doi.org/10.5281/zenodo.7474635 or also upon request (erik.johnson@postgrad.otago.ac.nz). Figures and data analysis untilised MATLAB Version 9.12.0 (R2022a) (The MathWorks Inc., 2022a), including the Mapping Toolbox (Version 5.3) (The MathWorks Inc., 2022b). Wind Roses were created using the Wind Rose function (Version 1.6.0.0) created by Daniel Pereira (https://www.mathworks.com/matlabcentral/fileexchange/47248-wind-rose).

Acknowledgments
We'd like to acknowledge the crucial work of Bill Dickson and Mark Elder on the Polaris II research vessel, in addition to the assistance of all staff and student researchers who have collected data along the Munida Transect through the years. This work is supported by the NZ Tertiary Education PBRF and a University of Otago Ph.D. Scholarship to E.E.J. The Munida Transect is supported by SIFF funding from the National Institute of Water and Atmospheric Research (NIWA) and strategic funding from the University of Otago. We are thankful for comments from anonymous reviewers, who improved the clarity and focus of this work. Open access publishing facilitated by University of Otago, as part of the Wiley - University of Otago agreement via the Council of Australian University Librarians.

References

Augé, A., Lalas, C., Davis, L., & Chilvers, B. (2012). Autumn diet of recolonising female New Zealand sea lions based at Otago Peninsula, South Island, New Zealand. *New Zealand Journal of Marine & Freshwater Research*, *46*(1), 97–110. https://doi.org/10.1080/00288330.2011.606326

Bodeker, G., Cullen, N., Katurji, M., McDonald, A., Morgenstern, O., Noone, D., et al. (2022). Aotearoa New Zealand climate change projections guidance: Interpreting the latest IPCC WG1 report findings (Technical report No. CR 501). Prepared for the Ministry for the Environment.

Boyd, P. W., LaRoche, J., Gall, M., Frew, R., & McKay, R. M. L. (1999). Role of iron, light, and silicate in controlling algal biomass in subantarctic waters SE of New Zealand. *Journal of Geophysical Research*, *104*(C6), 13395–13408. https://doi.org/10.1029/1999JC900009

Boyd, P. W., McTainsh, G., Sherlock, V., Richardson, K., Nichol, S., Ellwood, M., & Frew, R. (2004). Episodic enhancement of phytoplankton stocks in New Zealand subantarctic waters: Contribution of atmospheric and oceanic iron supply: Iron supply to subantarctic waters. *Global Biogeochemical Cycles*, *18*(1). https://doi.org/10.1029/2002GB002020

Brink, K. (2016). Cross-shelf exchange. *Annual Review of Marine Science*, *8*(1), 59–78. https://doi.org/10.1146/annurev-marine-010814-015717

Carranza, M. M., & Gille, S. T. (2015). Southern Ocean wind-driven entrainment enhances satellite chlorophyll-a through the summer. *Journal of Geophysical Research: Oceans*, *120*(1), 304–323. https://doi.org/10.1002/2014JC010203

Carranza, M. M., Gille, S. T., Piola, A. R., Charo, M., & Romero, S. I. (2017). Wind modulation of upwelling at the shelf-break front off Patagonia: Observational evidence: Wind modulation of shelf-break upwelling. *Journal of Geophysical Research: Oceans*, *122*(3), 2401–2421. https://doi.org/10.1002/2016JC012059

Childers, A. R., Whitledge, T. E., & Stockwell, D. A. (2005). Seasonal and interannual variability in the distribution of nutrients and chlorophyll a across the Gulf of Alaska shelf: 1998–2000. *Deep Sea Research Part II: Topical Studies in Oceanography*, *52*(1–2), 193–216. https://doi.org/10.1016/j.dsr2.2004.09.018

Chiswell, S. M. (1996). Variability in the Southland current, New Zealand. *New Zealand Journal of Marine & Freshwater Research*, *30*(1), 1–17. https://doi.org/10.1080/00288330.1996.9516693

Chiswell, S. M., Bradford-Grieve, J., Hadfield, M. G., & Kennan, S. C. (2013). Climatology of surface chlorophyll *a*, autumn-winter and spring blooms in the southwest Pacific ocean: Surface chlorophyll in southwest PACIFIC. *Journal of Geophysical Research: Oceans*, *118*(2), 1003–1018. https://doi.org/10.1002/jgrc.20088

Costello, M. J., & Chaudhary, C. (2017). Marine biodiversity, biogeography, deep-sea gradients, and conservation. *Current Biology*, *27*(11), R511–R527. https://doi.org/10.1016/j.cub.2017.04.060

Currie, K. I., Reid, M. R., & Hunter, K. A. (2011). Interannual variability of carbon dioxide drawdown by subantarctic surface water near New Zealand. *Biogeochemistry*, *104*(1–3), 23–34. https://doi.org/10.1007/s10533-009-9355-3

Davison, A. C., & Hinkley, D. V. (1997). *Bootstrap methods and their application*. Cambridge University Press.

du Plessis, M., Swart, S., Ansorge, I. J., & Mahadevan, A. (2017). Submesoscale processes promote seasonal restratification in the subantarctic ocean. *Journal of Geophysical Research: Oceans*, *122*(4), 2960–2975. https://doi.org/10.1002/2016JC012494

Eppley, R. W., Rogers, J. N., & McCarthy, J. J. (1969). Half-saturation constants for uptake of nitrate and ammonium by marine phytoplankton1. *Limnology and Oceanography*, *14*(6), 912–920. https://doi.org/10.4319/lo.1969.14.6.0912

Ferreira, A. S. A., Hátún, H., Counillon, F., Payne, M. R., & Visser, A. W. (2015). Synoptic-scale analysis of mechanisms driving surface chlorophyll dynamics in the North Atlantic. *Biogeosciences*, *12*(11), 3641–3653. https://doi.org/10.5194/bg-12-3641-2015

Fox-Kemper, B., Ferrari, R., & Hallberg, R. (2008). Parameterization of mixed layer eddies. Part I: Theory and diagnosis. *Journal of Physical Oceanography*, *38*(6), 1145–1165. https://doi.org/10.1175/2007JPO3792.1

Franks, P. J. S. (2001). Phytoplankton blooms in a fluctuating environment: The roles of plankton response time scales and grazing. *Journal of Plankton Research*, *23*(12), 1433–1441. https://doi.org/10.1093/plankt/23.12.1433

Franks, P. J. S., & Walstad, L. J. (1997). Phytoplankton patches at fronts: A model of formation and response to wind events. *Journal of Marine Research*, *55*(1), 1–29. https://doi.org/10.1357/0022240973224472

Hersbach, H., Bell, B., Berrisford, P., Biavati, G., Horányi, A., Muñoz Sabater, J., et al. (2023). ERA5 hourly data on single levels from 1940 to present. [Dataset]. Copernicus Climate Change Service (C3S) Climate Data Store (CDS). https://doi.org/10.24381/cds.adbb2d47

Hersbach, H., Bell, B., Berrisford, P., Hirahara, S., Horányi, A., Muñoz-Sabater, J., et al. (2020). The ERA5 global reanalysis. *Quarterly Journal of the Royal Meteorological Society*, *146*(730), 1999–2049. https://doi.org/10.1002/qj.3803

Hopkins, J., Palmer, M. R., Poulton, A. J., Hickman, A. E., & Sharples, J. (2021). Control of a phytoplankton bloom by wind-driven vertical mixing and light availability. *Limnology & Oceanography*, *66*(5), 1926–1949. https://doi.org/10.1002/lno.11734

Hopkins, J., Shaw, A., & Challenor, P. (2010). The Southland front, New Zealand: Variability and ENSO correlations. *Continental Shelf Research*, *30*(14), 1535–1548. https://doi.org/10.1016/j.csr.2010.05.016

IMOS. (2022). Imos - SRS - SST - L3S - single sensor - 1 day - day and night time - Australia. [Dataset]. Australian Ocean Data Network. Retrieved from https://portal.aodn.org.au

Jillett, J. B. (1969). Seasonal hydrology of waters off the Otago peninsula, South-Eastern New Zealand. *New Zealand Journal of Marine & Freshwater Research*, *3*(3), 349–375. https://doi.org/10.1080/00288330.1969.9515303

Jones, K. N., Currie, K. I., McGraw, C. M., & Hunter, K. A. (2013). The effect of coastal processes on phytoplankton biomass and primary production within the near-shore Subtropical Frontal Zone. *Estuarine, Coastal and Shelf Science*, *124*, 44–55. https://doi.org/10.1016/j.ecss.2013.03.003

Kidson, J. W. (2000). An analysis of New Zealand synoptic types and their use in defining weather regimes. *International Journal of Climatology*, *20*(3), 299–316. https://doi.org/10.1002/(SICI)1097-0088(20000315)20:3〈299::AID-JOC474〉3.0.CO;2-B

Leathwick, J., Elith, J., Francis, M., Hastie, T., & Taylor, P. (2006). Variation in demersal fish species richness in the oceans surrounding New Zealand: An analysis using boosted regression trees. *Marine Ecology Progress Series*, *321*, 267–281. https://doi.org/10.3354/meps321267

Lévy, M., Mémery, L., & Madec, G. (2000). Combined effects of mesoscale processes and atmospheric high-frequency variability on the spring bloom in the MEDOC area (p. 27).

Long, M. C., Thomas, L. N., & Dunbar, R. B. (2012). Control of phytoplankton bloom inception in the Ross Sea, Antarctica, by Ekman restratification: Ekman restratification in the Ross Sea. *Global Biogeochemical Cycles*, *26*(1). https://doi.org/10.1029/2010GB003982

Longhurst, A. R. (2007). *Ecological geography of the sea* (2nd ed.). Elsevier.

Mahadevan, A., D'Asaro, E., Lee, C., & Perry, M. J. (2012). Eddy-driven stratification initiates north Atlantic spring phytoplankton blooms. *Science*, *337*(6090), 54–58. https://doi.org/10.1126/science.1218740

McGill, R., Tukey, J. W., & Larsen, W. A. (1978). Variations of box plots. *The American Statistician*, *32*(1), 12. https://doi.org/10.2307/2683468

Mitchell, J., Mackay, K., Neil, H., Mackay, E., Pallentin, A., & Notman, P. (2012). Undersea New Zealand [NIWA chart].

Murphy, R. J., Pinkerton, M. H., Richardson, K. M., Bradford-Grieve, J. M., & Boyd, P. W. (2001). Phytoplankton distributions around New Zealand derived from SeaWiFS remotely-sensed ocean colour data. *New Zealand Journal of Marine & Freshwater Research*, *35*(2), 343–362. https://doi.org/10.1080/00288330.2001.9517005

Oliver, H., Zhang, W. G., Archibald, K. M., Hirzel, A. J., Smith, W. O., Sosik, H. M., et al. (2022). Ephemeral surface chlorophyll enhancement at the New England shelf break driven by Ekman restratification. *Journal of Geophysical Research: Oceans*, *127*(1). https://doi.org/10.1029/2021JC017715

Paltoglou, G., Beggs, H., & Majewski, L. (2010). New AUSTRALIAN high resolution AVHRR SST products from the integrated marine observing system (p. 11).

Sathyendranath, S., Brewin, R. J. W., Brockmann, C., Brotas, V., Calton, B., Chuprin, A., et al. (2019). An Ocean-colour time series for use in climate studies: The experience of the ocean-colour climate change initiative (OC-CCI) (p. 31).

Sathyendranath, S., Jackson, T., Brockmann, C., Brotas, V., Calton, B., Chuprin, A., et al. (2021). ESA Ocean Colour climate change initiative (Ocean_colour_cci): Version 5.0 data. [Dataset]. NERC EDS Centre for Environmental Data Analysis. https://doi.org/10.5285/1DBE7A109C0244AAAD713E078FD3059A

Sharmar, V., & Markina, M. (2020). Validation of global wind wave hindcasts using ERA5, MERRA2, ERA-Interim and CFSRv2 reanalyzes. *IOP Conference Series: Earth and Environmental Science*, *606*(1), 012056. https://doi.org/10.1088/1755-1315/606/1/012056

Siedlecki, S. A., Archer, D. E., & Mahadevan, A. (2011). Nutrient exchange and ventilation of benthic gases across the continental shelf break. *Journal of Geophysical Research*, *116*(C6), C06023. https://doi.org/10.1029/2010JC006365

Siegel, D. A., Doney, S. C., & Yoder, J. A. (2002). The North Atlantic spring phytoplankton bloom and Sverdrup's critical depth Hypothesis. *Science*, *296*(5568), 730–733. https://doi.org/10.1126/science.1069174

Sturman, A. P., Trewinnard, A. C., & Gorman, P. A. (1984). A study of atmospheric circulation over the South Island of New Zealand (1961-1980). *Weather and Climate*, *4*(2), 53. https://doi.org/10.2307/44279622

Taylor, J. R., & Ferrari, R. (2011). Shutdown of turbulent convection as a new criterion for the onset of spring phytoplankton blooms. *Limnology and Oceanography*, *56*(6), 2293–2307. https://doi.org/10.4319/lo.2011.56.6.2293

The MathWorks Inc. (2022a). MATLAB version: 9.12.0 (R2022a). Natick, Massachusetts: The MathWorks Inc. Retrieved from https://www.mathworks.com

The MathWorks Inc. (2022b). Mapping Toolbox version: 5.3 (R2022b). Natick, Massachusetts: The MathWorks Inc. Retrieved from https://www.mathworks.com

Thomas, L. N., & Lee, C. M. (2005). Intensification of ocean fronts by down-front winds. *Journal of Physical Oceanography*, *35*(6), 1086–1102. https://doi.org/10.1175/JPO2737.1

Vincent, W. F., Howard-Williams, C., Tildesley, P., & Butler, E. (1991). Distribution and biological properties of oceanic water masses around the South Island, New Zealand. *New Zealand Journal of Marine & Freshwater Research*, *25*(1), 21–42. https://doi.org/10.1080/00288330.1991.9516451

Watson, R., Kitchingman, A., Gelchu, A., & Pauly, D. (2004). Mapping global fisheries: Sharpening our focus. *Fish and Fisheries*, *5*(2), 168–177. https://doi.org/10.1111/j.1467-2979.2004.00142.x

Whitt, D. B., Lévy, M., & Taylor, J. R. (2017). Low-frequency and high-frequency oscillatory winds synergistically enhance nutrient entrainment and phytoplankton at fronts: WIND, fronts, and phytoplankton. *Journal of Geophysical Research: Oceans*, *122*(2), 1016–1041. https://doi.org/10.1002/2016JC012400

Xu, Y., Chant, R., Gong, D., Castelao, R., Glenn, S., & Schofield, O. (2011). Seasonal variability of chlorophyll a in the mid-Atlantic Bight. *Continental Shelf Research*, *31*(16), 1640–1650. https://doi.org/10.1016/j.csr.2011.05.019

Zarubin, M., Lindemann, Y., & Genin, A. (2017). The dispersion-confinement mechanism: Phytoplankton dynamics and the spring bloom in a deeply-mixing subtropical sea. *Progress in Oceanography*, *155*, 13–27. https://doi.org/10.1016/j.pocean.2017.05.005